CASE FILE
COPY

NACA TN No. 1700

NATIONAL ADVISORY COMMITTEE FOR AERONAUTICS

Corrected copy

TECHNICAL NOTE

No. 1700

THE ROLLING MOMENT DUE TO SIDESLIP OF TRIANGULAR, TRAPEZOIDAL, AND RELATED PLAN FORMS IN SUPERSONIC FLOW

By Arthur L. Jones, John R. Spreiter,
and Alberta Alksne

Ames Aeronautical Laboratory,
Moffett Field, Calif.

Washington
October 1948

PROPERTY FAIRCHILD
ENGINEERING LIBRARY

NATIONAL ADVISORY COMMITTEE FOR AERONAUTICS

TECHNICAL NOTE NO. 1700

THE ROLLING MOMENT DUE TO SIDESLIP OF TRIANGULAR, TRAPEZOIDAL, AND RELATED PLAN FORMS IN SUPERSONIC FLOW

By Arthur L. Jones, John R. Spreiter, and Alberta Alksne

SUMMARY

The rolling moment due to sideslip in supersonic flow has been calculated for a representative group of plan forms. The analysis was based on linearized potential theory and was applied to triangular, trapezoidal, rectangular, and swept-back plan forms without dihedral.

The only types of plan forms that provided positive dihedral effect throughout the range of Mach number investigated were the rectangular wing of very low aspect ratio and a trapezoidal wing of moderately low aspect ratio having raked-out tips.

The variation of rolling moment with sideslip was found to be linear over a small range of sideslip angles for practically all the Mach cone plan-form configurations investigated.

INTRODUCTION

The calculation of the supersonic lateral-stability derivatives has been undertaken for a group of plan forms of the type shown in figures 1 and 2 considered to be representative of the plan forms proposed for flight at supersonic speeds. In reference 1 the results for the damping-in-roll derivatives were presented. This report extends the results to include the rolling moment due to sideslip.

The load distributions for the sideslipping wings were obtained using the methods presented in references 1, 2, 3, and 4. The load

distributions were then integrated to obtain the rolling-moment coefficient as a function of sideslip.

In general, the plan forms may be described as: (1) triangular with subsonic leading edges and with supersonic leading edges; (2) trapezoidal with all possible combinations of raked-in, raked-out, subsonic or supersonic tips; (3) rectangular; and (4) two swept-back plan forms with supersonic trailing edges developed from the triangular wings. A small change has been made in one of the plan forms under investigation since reference 1 was published. In reference 1, the swept-back plan form having subsonic leading edges was developed by removing a small triangular portion, having sides parallel to the Mach cones, from the trailing edge of a triangular plan form having subsonic leading edges. Due to the difficulties encountered in analyzing the sideslip position for this particular configuration, the portion removed from the basic triangular plan form has been changed. A triangular section extending from tip to tip is now removed leaving the wing tapered to a point at the tip as shown in figure 2.

Previous work on wings in sideslip has been reported in references 5, 6, 7, 8, and 9.

SYMBOLS AND COEFFICIENTS

x,y	rectangular coordinates of wind axes
ξ,η	rectangular coordinates of body axes
V	free-stream velocity
b	span of wing measured normal to plane of symmetry
c_r	root chord of wing
l	over-all longitudinal length of swept-back wing
S	area of wing
A	aspect ratio $\left(\frac{b^2}{S}\right)$
ρ	density in the free stream
q	free-stream dynamic pressure $\left(\frac{\rho}{2}V^2\right)$

M_ξ rolling moment about longitudinal body axes (positive for right wing rolling down)

C_l rolling-moment coefficient $\left(\frac{M_\xi}{qSb}\right)$

L lift

β sideslip angle, degrees (positive when sideslipping to right)

C_{l_β} rolling-moment-due-to-sideslip stability derivative $\left(\frac{\partial C_l}{\partial \beta}\right)$

M_1 free-stream Mach number

B $\sqrt{M_1^2-1}$

μ Mach angle (arc tan $\frac{1}{B}$)

m slope of right wing tip measured from line parallel to plane of symmetry in plane of wing (positive for raked-out tip, negative for raked-in tip)

Bm $\frac{m}{\tan \mu}$, ratio of tangent of right tip angle to tangent of Mach cone angle

$F(\varphi,k)$ incomplete elliptic integral of the first kind with modulus k

$E(\varphi,k)$ incomplete elliptic integral of the second kind with modulus k

α angle of attack, radians

METHODS

The problem of determining the load distribution on a wing in sideslip is essentially the problem of determining the loading on an inclined flat plate. The fact that the plane of symmetry of the plan form is not alined with the free-stream direction does not greatly affect the analysis. The methods used in reference 1, therefore were applicable again.

The load distribution on the triangular and trapezoidal plan-form configurations, having supersonic edges entirely, were determined readily by the source-sink and doublet method of reference 2. The loading on an area affected by a subsonic edge in conjunction with a supersonic leading edge or tip was obtained by a simple direct integration using the method of reference 3 with the stipulation that the Kutta condition must be satisfied on all subsonic trailing edges as provided for in reference 4. The triangular plan form with subsonic leading edges has been analyzed previously in the sideslip position and the load distribution is available in reference 8. The method followed in reference 8 was used to determine the loading on the subsonic-edged triangular plan form lying between one edge of the Mach cone and the cone axis. In reference 6, also, the expression for the load distribution on this plan form is presented.

The plan forms were divided into sectors, bounded by the plan-form edges and the Mach cone traces, in order to simplify the analysis and the presentation of the results. Lift and moment expressions were obtained for these sectors by integration of the load distributions. In Appendix A, the formulas for the moments of the complete plan forms are expressed in symbols representing the moment and lift expressions of the plan-form sectors or combinations of these sectors. These expressions which do not readily combine and simplify are given in Appendix B.

Another condition that required the simplification of the presentation of the moment expressions for a complete plan form was the change in Mach cone configuration that a wing in sideslip undergoes in supersonic flow. As the tips change from subsonic to supersonic or vice versa, and as the edges and tips change figuratively from leading to trailing edges by swinging past the free-stream direction, the load distribution and rolling moment change considerably. Consequently, it was necessary to divide the sideslip rotation into a number of phases in order that an expression for the rolling moment could be provided for each configuration encountered in the range of sideslip investigated.

The determination of an analytical form for C_{l_β} by differentiation of the expression for C_l as a function of β was found to be impractical. Linearity of the C_l variation with β for a small range of sideslip angles, however, made it convenient to calculate a value of the derivative based on the value for C_l at 5° of sideslip. This approximation is more fully explained in the discussion of the results.

The plan forms are classified with regard to the relative positions of the wing tips and the tip Mach cones when the wing is at zero sideslip. The ratio of the tangent of the right tip angle to the tangent of the Mach cone angle Bm makes a convenient index. The slope of the right tip m is defined as positive when the tip is raked out and negative when the tip is raked in. If Bm is equal to or greater than 1, the tips are supersonic leading edges. If Bm is equal to or less than −1, the tips are supersonic trailing edges. For values of Bm between 1 and −1, the tips are subsonic.

DISCUSSION OF RESULTS

The general results are the rolling-moment-coefficient formulas given in Appendix A for all the plan forms considered. For a practical interpretation of the results, a number of typical plan forms have been selected for which the rolling-moment coefficient was calculated. These results are presented in graphical form in figures 3 through 9. Included in Appendix A are expressions for the values of tan β that mark the phase changes and for the value of tan β representing a span limitation. The existence of a span limitation is due to the difficulty in obtaining an expression for the load distribution when the Mach cone from one tip reflects off the other tip. The degree of sideslip is limited also by restricting the Mach cone originating at the juncture of the trailing edge and the tip from overlapping the wing. This limitation, $\tan \beta \leq B$, applies to all plan forms. Other limitations that were required for the swept-back plan-form configurations are explained when they are presented.

It should be pointed out that for the swept-back plan-form configurations the phases given do not cover the utmost sideslip angle to which the analysis could have been carried. For the rest of the plan forms, expressions are given to cover the utmost possible sideslip angle that this analysis permitted. In most cases, this represents a magnitude of sideslip angle far beyond what normally is interesting and useful. In view of the length and complexity of the analyses for the swept-back wings, however, the sideslip angles considered for these plan forms were held to a minimum.

Variation of $\frac{C_l}{\alpha}$ with β

The variation of rolling-moment coefficient per unit angle of attack with sideslip angle for the specific plan forms considered

are shown in figures 3 and 4 for two values of B (1 and $\frac{4}{3}$). If a negative slope corresponding to positive dihedral effect is defined as a stable variation of C_l with β, it is evident that more plan forms had unstable than stable variations. The breaks in the curves are due to changes in phase that occur as the wing progresses in sideslip. In some cases where the tip is raked out, the breaks reversed the variation of C_l with β from unstable to stable or vice versa.

It is evident, from the expressions for the moments and from the curves showing the variation of C_l with β, that C_l is not a linear function of sideslip and no simple expressions are obtainable for the derivative C_{l_β}. For the values of B considered in figures 3 and 4, however, the variation of C_l with β is very close to linear for the first 10° of sideslip. To obtain an indication as to the effects of aspect ratio and Mach number on the variation of roll in sideslip for the plan forms considered, therefore, it was assumed that a linear derivative could be established for at least the first 5° of sideslip. In figures 5 through 9, this derivative is shown plotted as a function of aspect ratio and as a function of the Mach number parameter B. The assumption of a constant slope was justified except at values of B where a phase change occurred within the first 5° of sideslip.

For the values of B at which the variation of C_l was determined to be nonlinear within the first 5° of sideslip, dotted lines represent the value of the derivative for whatever sideslip range the linearity existed. At the values of B for which, at zero sideslip, the Mach cones and the tips are nearly coincident, a value of C_{l_β} based on the C_l at 5° of sideslip was determined. This value of C_{l_β} did not truly represent the slope of the C_l curve because a phase change and a break in the curve occurs within the first 5° of sideslip. This psuedo derivative is plotted as a continuation of the solid curve in the regions where the dotted curves exist. Its principal value is that it shows whether the slope increases or decreases in magnitude in passing from the first to the second phase. At the value of B for which the Mach cone and the tip are exactly coincident, the slope of C_l with β is constant for a range of sideslip greater than 5°. This point lies on the solid curve at the value of B where the discontinuity in the dotted branches exist.

The property of reversibility, whereby a given plan form provides the same lift, drag, or damping in roll whether or not the plan form was reversed with respect to the stream direction,

did not occur in the rolling-moment-due-to-sideslip derivative. Apparently the lack of symmetry about the wind axes that results from the sideslip prohibits the realization of reversibility in this case.

Variation of $\frac{C_{l_\beta}}{\alpha}$ with Aspect Ratio

The variation of C_{l_β} per unit angle of attack with aspect ratio presented in figure 5 for values of B equal to 1 and $\frac{4}{3}$ shows that for the most part the magnitude of the derivatives decreases with increasing aspect ratio. For the trapezoids with subsonic raked-out tips, the derivative is stable and this reduction exists throughout the entire range of aspect ratio investigated; whereas the values for the supersonic-tipped trapezoidal plan forms have gone from stable to unstable and increased in magnitude with increasing aspect ratio.

As a trapezoidal plan form is reduced in span, it eventually becomes a triangular plan form. This transition occurs at an aspect ratio of 4m. If a triangular plan form is developed by reducing the span of one of the supersonic raked-out-tip trapezoidal plan forms shown, the value of the derivative changes suddenly from stable to unstable. As the aspect ratio is reduced farther, necessarily reducing the slope of the edge of the triangular plan form, the magnitude of the unstable derivative becomes greater and then suddenly jumps to a stable value as the leading edges of the triangle become subsonic at an aspect ratio of $\frac{4}{B}$. As the aspect ratio of the triangular wings approaches zero, the values of $C_{l\beta}$ approach a value slightly higher than the value given by Ribner (-0.0183, in reference 9) for low-aspect-ratio triangular wings. If the sideslip angle for determining C_{l_β} were allowed to approach zero rather than to remain equal to 5°, the C_{l_β} curve would approach the value given by Ribner.

For all but a small range of aspect ratios at the lower end of the aspect ratio scale, the rectangular and the trapezoidal plan forms with subsonic raked-in tips show a decreasing magnitude for C_{l_β} with increasing aspect ratio. The trapezoidal plan forms with supersonic raked-in tips have derivatives equal to zero because at $B = 1$ and $B = \frac{4}{3}$ the tip Mach cones lie farther than 5° away from the tips, and the load distribution is uniform yielding zero rolling moment for these plan forms until one tip crosses one of

the tip Mach cones. The value of the derivative remains zero when this plan form has been reduced to an inverted triangular plan form. Further reduction in aspect ratio requires a reduction in the slope of the tips of the triangle which eventually leads to a phase change and to the existence of a rolling moment due to sideslip within the first 5° of sideslip. This inverted type of triangular plan form cannot be investigated below an aspect ratio of $\frac{4}{B}$ because the tip Mach cones reflect on the opposite edges. For the same reason, the trapezoids with subsonic raked-in tips cannot be analyzed if reduced to triangular plan forms.

As indicated previously, the rectangular plan form and the trapezoidal plan forms with subsonic raked-in tips have a critical value of aspect ratio at which the unstable value for C_{l_β} stops increasing in magnitude as aspect ratio is decreasing and tends to become less unstable. For the rectangular plan form, this reversal of trend occurs at an aspect ratio equal to $\frac{6+4B^2}{3B}$ which is greater than the aspect ratio at which the tip Mach cones crossed at the trailing edge $\left(A = \frac{B}{2}\right)$. The rectangular wings were amenable to analysis at Mach numbers low enough $(1 < AB < 2)$ to show that this trend eventually yielded stable values for the derivative. The aspect ratio at which the change from unstable to stable values occurs is half the aspect ratio at which the curve starts to reverse its trend, that is, when $A = \frac{3+2B^2}{3B}$. From this expression it can shown that there is a minimum aspect ratio of 1.635 at which the change in the sign of the dihedral effect occurs. The value of B that produces this minimum is $\sqrt{3/2}$. At these values, the reversal of sign and the crossing of the tip Mach cones occur simultaneously. For values of B greater than $\sqrt{3/2}$, the reversal of dihedral effect occurs at an aspect ratio greater than the aspect ratio at which the tip Mach cones cross. This order of occurrence is reversed if B is less than $\sqrt{3/2}$.

The variation of C_{l_β} with aspect ratio for the swept-back plan forms considered is shown in figure 6. For the subsonic-edged plan forms, the trend was toward more stable values of the derivative as the aspect ratio increased. For the supersonic-edged swept-back plan forms, the trend was toward more unstable values of the derivative as the aspect ratio increased. Thus the swept-back plan forms were

the only ones for which C_{l_β} increased in magnitude with an increase in aspect ratio.

Variation of $\frac{C_{l_\beta}}{\alpha}$ with B

The variation of C_{l_β} per unit angle of attack with B shown in figures 7, 8, and 9 is the most useful curve for determining the suitability of any plan form with regard to roll-in-sideslip stability. With two exceptions, the values of the derivatives shown on this curve establish the stable or unstable sense of the variation of C_l with β that exists for the entire sideslip range for a given plan form at a given speed. The exceptions to this rule are the triangular plan form with supersonic tips and the supersonic trapezoidal plan forms with raked-out tips.

In general, the C_{l_β} curves are approaching zero at the upper end of the B scale for all the plan forms. At the lower end of the B scale, the curves tend toward either very large positive or negative values of C_{l_β}. The curves are considered in greater detail in the following discussion of the individual plan forms.

Triangular plan forms: Tips raked out, $m = \frac{1}{2}$, $m = \frac{3}{2}$.- At the lower end of the B scale, all of the triangular plan forms have subsonic tips. In this configuration, both of the triangular wings considered, aspect ratio 6 in figure 7 and aspect ratio 2 in figure 9, have fairly large stable values of C_{l_β}. With increasing values of B, however, the Mach cone approaches the leading edge and crosses it and, in this range of B, C_{l_β} drops from the relatively large stable value to an unstable value. The value of C_{l_β} for this supersonic-tipped configuration then decreases as B is increased and tends to approach zero asymptotically.

Triangular plan forms: Tips raked in, $m = -\frac{1}{2}$, $m = -\frac{3}{2}$.- At the lower values of B, the tip Mach cones overlap these inverted triangular plan forms, and the reflections of the Mach lines from tip to tip constitute a configuration that does not permit the formulation of loading and moment expressions in closed form. When the Mach number has increased until the Mach cones are coincident with the sides of the triangle, a closed form of expression for the load distribution and moment can be obtained. At this point, the first phase extends to considerably more than 5°

and an unstable value of C_{l_β} is obtained as shown in figure 7 for aspect ratio 6. This instability drops off rapidly and reaches zero when B has increased to the point where the Mach cones fall at least 5° outside the tips. For sideslip angles greater than 5°, the variation of C_l with β (figs. 3 and 4) shows that when the sideslip angle reaches the second phase the zero value for the derivative changes to an unstable variation of roll in sideslip.

Rectangular plan forms.- The variation of C_{l_β} with B for the rectangular plan forms is quite dependent on aspect ratio. Below the aspect ratio of 1.635 (as discussed previously with regard to the variation of C_{l_β} with regard to aspect ratio) the rectangular plan form gives positive dihedral effect throughout the Mach number range investigated as shown in figure 7(a) for an aspect ratio of 1.5. As the aspect ratio increases, the curve showing the C_{l_β} variation with B crosses into the unstable region at a fairly low value of B but recrosses to the stable side at a higher value. As the aspect ratios become fairly large (A = 6 and A = 9 in figs. 7(b) and 8), the values of B for crossing become so small and the values for recrossing become so large that for the range of Mach numbers considered the curve seems to lie entirely in the unstable region.

Trapezoidal plan forms: Tips raked out, $m = \frac{1}{2}$.- These trapezoidal plan forms show somewhat the same characteristics as the rectangular plan form in regard to the reversal in the stability of the roll due to sideslip that occurs at about the time the tip Mach cones cross at the trailing edge. At the lower end of the B scale in figure 7(a), the curve for the aspect ratio 4 plan form tends toward infinity in the stable derivative zone after completely reversing its trend toward the unstable zone from B = 1 to $B = \frac{1}{2}$. At aspect ratios of 6 and 9, however, the curves shown in figures 7(b) and 8 have crossed the C_{l_β} axis and are heading toward large positive values at the lower end of the B scale. Above the value B = 1, the curves for all three aspect ratios follow parallel patterns. The magnitude of C_{l_β} decreases as the Mach cones approach the tip and, as the tips become supersonic, continue to decrease finally approaching zero asymptotically at the upper end of the B scale. The variation of roll in sideslip was stable at all times for B greater than 1.

Trapezoidal plan forms: Tips raked out, $m = \frac{3}{2}$.- The aspect ratio 6 with $m = \frac{3}{2}$ is a triangular plan form. Above an aspect ratio of 6, however, the plan forms having $m = \frac{3}{2}$ are trapezoids. At the aspect ratio of 9 shown if figure 8, the curve lies almost entirely in the unstable region. At the aspect ratio of 6.5, shown in figure 7 (a), the curve lies mostly in the stable region except for the dip into the unstable region near $B = 1$. The variation of C_{l_β} with aspect ratio shown in figure 5 indicates that at an aspect ratio of approximately 6.2 the derivative is stable for $B = 1$ and $B = \frac{4}{3}$ and, therefore, it is quite probable that the curve for a trapezoidal plan form of this aspect ratio might lie entirely in the stable range.

Trapezoidal plan forms: Tips raked in, $m = -\frac{1}{2}$.- These trapezoidal plan forms have no essential differences in the pattern of their C_{l_β} variation with B for aspect ratios 6 and 9. These curves are presented in figures 7 and 8. The pattern of the variation is similar to the variation of C_{l_β} with B for the rectangular plan forms of aspect ratios 6 and 9, tending toward large unstable values of C_{l_β} at the lower end of the B scale and dropping off in magnitude as B increases. The sudden drop to $C_{l_\beta} = 0$ occurs when the tips have become supersonic.

For values of aspect ratio considerably lower than 6, where the tip crossing effect might become appreciable again, it is quite likely that C_{l_β} would tend to become stable at the lower end of the B scale.

Trapezoidal plan forms: Tips raked in, $m = -\frac{3}{2}$.- At an aspect ratio of 6, the plan-form shape for $m = -\frac{3}{2}$ is triangular, but for aspect ratios of greater than 6 the plan form becomes trapezoidal. At the lower end of the B scale in figure 8, where the trapezoidal plan form of aspect ratio 9 has subsonic tips, the roll-in-sideslip variation is unstable as it was for the triangular plan form of aspect ratio 6. As B increases and the tips become supersonic by passing through the Mach cone, the value of C_{l_β} based on C_l at a sideslip angle of 5° is zero. If the angle of sideslip is increased

till the second phase is reached, however, the variation of C_l with β is unstable.

Swept-back plan forms: Subsonic edges, $m = \frac{1}{2}$.- Over the limited range of B's for which the computation of C_{l_β} was possible, the results indicated that C_{l_β} decreases with an increase in B. The magnitude of the derivatives for this plan form was greater than the magnitude of the derivatives for the triangular plan form with the same edge slopes.

Swept-back plan forms: Supersonic edges, $m = \frac{3}{2}$, $m = \frac{1}{2}$.- As for the subsonic-edged swept-back plan forms, the magnitude of the derivative was greater than the magnitude for the corresponding triangle and the variation of the derivative with B showed that within the first phase increasing B reduced the magnitude of the derivative.

CONCLUDING REMARKS

The variation of rolling-moment coefficient with sideslip was found to be approximately linear over a small range of sideslip angles for the plan forms investigated. Both positive and negative dihedral effects were obtained.

For a given plan-form type and a given tip or leading-edge classification (subsonic or supersonic), derivatives evaluated for the linear range of the C_l variation with β were generally found to decrease in magnitude with increasing aspect ratio. The outstanding exception to this generalization was the swept-back plan form with either subsonic or supersonic leading edges.

The rectangular plan forms of very low aspect ratio ($A < 1.635$) and the trapezoidal plan forms of moderately low aspect ratio ($A \approx 4$) with raked-out tips apparently are the most satisfactory plan forms for providing positive dihedral effect. At the larger aspect ratios, these two plan forms provided negative dihedral effect over at least part of the Mach number range. The triangular plan forms and the swept-back plan forms provided positive dihedral effect as long as their leading edges remained subsonic but changed to negative dihedral effect when the leading edges became supersonic. The trapezoidal plan forms with raked-in tips yielded negative dihedral effect with subsonic tips, but achieved zero dihedral effect over

a limited sideslip range when the tips became supersonic. The general trend of the variation of C_{l_β} with Mach number was a reduction in the magnitude of the derivative with an increase in Mach number.

Ames Aeronautical Laboratory,
National Advisory Committee for Aeronautics,
Moffett Field, Calif.

APPENDIX A

FORMULAS FOR ROLLING MOMENT DUE TO SIDESLIP
General Restriction: $\tan \beta \leq B$

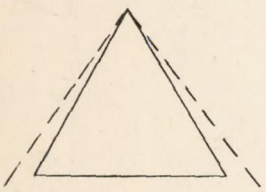
TRIANGULAR WINGS

Subsonic Tips

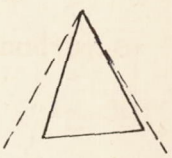
$Bm < 1$

$$C_l = \frac{M_\xi}{qSb} = \frac{M_\xi}{2qc_r{}^3m^2}$$

$$m \geq \frac{1}{B+\sqrt{B^2+1}}$$



Phase 1, $0 \leq \tan \beta \leq \left(\frac{1-Bm}{B+m}\right)$



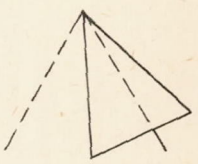
$$M_\xi = M_A$$

Phase 2, $\left(\frac{1-Bm}{B+m}\right) \leq \tan \beta \leq m$



$$M_\xi = M_C$$

Phase 3, $m \leq \tan \beta \leq \left(\frac{1+Bm}{B-m}\right)$



$$M_\xi = M_D$$

$$m < \frac{1}{B+\sqrt{B^2+1}}$$

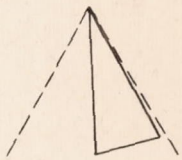


Phase 1, $0 \leq \tan \beta \leq m$



$$M_\xi = M_A$$

Phase 2, $m \leq \tan \beta \leq \left(\frac{1-Bm}{B+m}\right)$



$$M_\xi = M_B$$

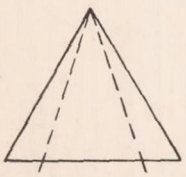
Phase 3, $\left(\frac{1-Bm}{B+m}\right) \leq \tan \beta \leq \left(\frac{1+Bm}{B-m}\right)$



$$M_\xi = M_D$$

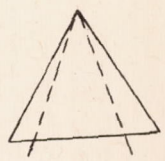
Supersonic Tips

$Bm \geq 1$



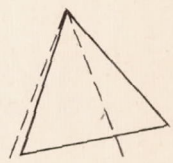
$$C_l = \frac{M_\xi}{qSb} = \frac{M_\xi}{2qc_r{}^3m^2}$$

Phase 1, $0 \leq \tan \beta \leq \left(\frac{Bm-1}{B+m}\right)$



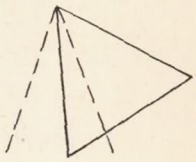
$$M_\xi = M_E$$

Phase 2, $\left(\frac{Bm-1}{B+m}\right) \leq \tan \beta \leq m$



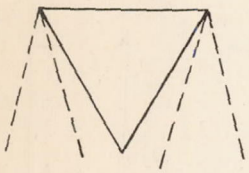
$$M_\xi = M_C$$

Phase 3, $m \leq \tan \beta \leq \left(\frac{1+Bm}{B-m}\right)$



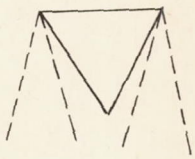
$$M_\xi = M_D$$

$Bm \leq -1$



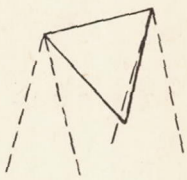
$$C_l = \frac{M_\xi}{qSb} = \frac{M_\xi}{2qc_r{}^3 m^2}$$

Phase 1, $0 \leq \tan \beta \leq -\left(\frac{Bm+1}{B-m}\right)$



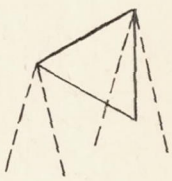
$$M_\xi = 0$$

Phase 2, $-\left(\frac{Bm+1}{B-m}\right) \leq \tan \beta \leq -m$



$$M_\xi = M_F$$

Phase 3, $-m \leq \tan \beta \leq \left(\frac{1-Bm}{B+m}\right)$



$$M_\xi = M_G$$

SWEPT-BACK WINGS

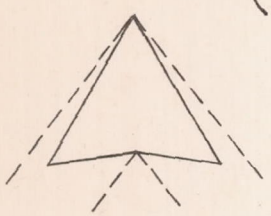
Subsonic Tips

$Bm < 1$

$$C_l = \frac{M_\xi}{qSb} = \frac{M_\xi}{q\,\frac{b^2 c_r}{2}}$$

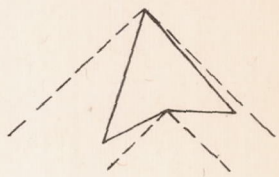
$$m \geq \frac{1}{B+\sqrt{B^2+1}}$$

$$0 \leq (l-c_r) \leq \frac{l(B^2+2Bm-1)}{\left(-B^2+2\frac{B}{m}+1\right)}$$



Phase 1, $0 \leq \tan \beta \leq \frac{1-Bm}{B+m}$

$$M_\xi = M_A - M_H$$



$$\frac{l(B^2+2Bm-1)}{\left(-B^2+2\frac{B}{m}+1\right)} \overset{a}{\leq} (l-c_r) \leq Bml^b$$



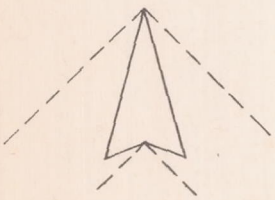
Phase 1, $0 \leq \tan \beta \leq \frac{Bl m-(l-c_r)}{B(l-c_r)+lm}$

$$M_\xi = M_A - M_H$$



$$m < \frac{1}{B+\sqrt{B^2+1}}$$

$$0 \leq (l-c_r) \leq \frac{l(B^2+2Bm-1)}{\left(-B^2+2\frac{B}{m}+1\right)}$$

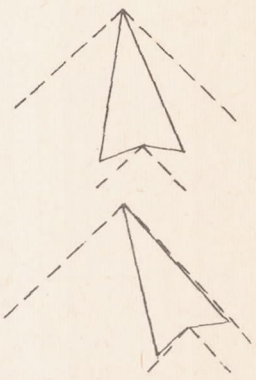


Phase 1, $0 \leq \tan \beta \leq m$

$$M_\xi = M_A - M_H$$

Phase 2, $m \leq \tan \beta \leq \frac{1-Bm}{B+m}$

$$M_\xi = M_B - M_I$$

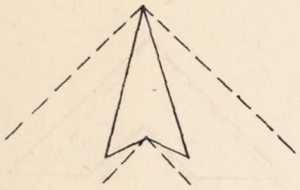


---

[a] Inside left edge hits Mach cone from cutout before right leading edge becomes supersonic.

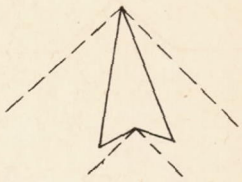
[b] Prevents Mach cone at cutout from crossing wing at zero sideslip.

$$\frac{l(B^2+2Bm-1)}{\left(-B^2+2\frac{B}{m}+1\right)}^{c} \leq (l-c_r) \leq lm \left(\frac{B-m}{Bm+1}\right)^{d}$$



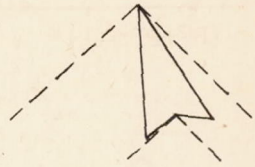
Phase 1, $0 \leq \tan \beta \leq m$

$$M_\xi = M_A - M_H$$

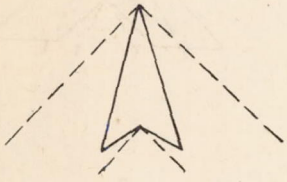


Phase 2, $m \leq \tan \beta \leq \frac{Blm-(l-c_r)}{B(l-c_r)+lm}$

$$M_\xi = M_B - M_I$$

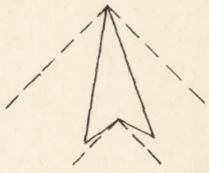


$$lm \left(\frac{B-m}{Bm+1}\right)^{e} \leq (l-c_r) \leq Bml$$



Phase 1, $0 \leq \tan \beta \leq \frac{Blm-(l-c_r)}{B(l-c_r)+lm}$

$$M_\xi = M_A - M_H$$



Supersonic Tips

$Bm \geq 1$

$$C_l = \frac{M_\xi}{qSb} = \frac{M_\xi}{qbm\left[l\left(\frac{b}{2m}+2c_r\right)-l^2-c_r{}^2\right]}$$

$$m < \frac{2B}{B^2-1}^{f}$$

---

[c] Inside left edge hits Mach cone from cutout before right leading edge becomes supersonic.

[d] Left leading edge swings past X-axis before inside left edge hits Mach cone from cutout.

[e] Inside left edge hits Mach cone from cutout before left leading edge swings past X-axis.

[f] Prevents ξ-axis from crossing Mach cone at right before left edge hits Mach cone.

$$0 \leq (l-c_r) \leq \frac{l\left(-B^2+\frac{2B}{m}+1\right)}{(B^2+2Bm-1)}$$

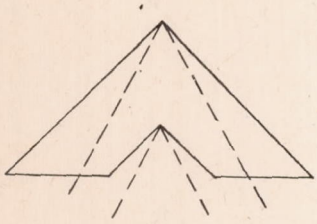


Phase 1, $0 \leq \tan \beta \leq \left(\frac{Bm-1}{B+1}\right)$



$$M_\xi = M_E - M_J$$

$$\frac{l\left(-B^2+\frac{2B}{m}+1\right)^{g}}{(B^2+2Bm-1)} \leq (l-c_r) \leq \frac{l^{h}}{mB}$$



Phase 1, $0 \leq \tan \beta \leq \frac{l-Bm(l-c_r)}{Bl+m(l-c_r)}$



$$M_\xi = M_E - M_J$$

Phase 2, $\frac{l-Bm(l-c_r)}{Bl+m(l-c_r)} \leq \tan \beta \leq \frac{Bm-1}{B+m}$



$$M_\xi = M_E - M_K$$

---

[g] Inside right edge hits apex Mach cone before left leading edge hits apex Mach cone.

[h] Prevents cutout from overlapping apex Mach cone at zero sideslip.

TRAPEZOIDAL WINGS

Subsonic tips

$0 > Bm > -1$

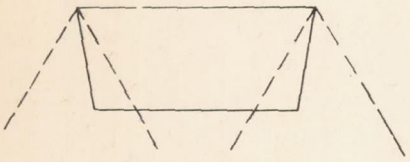
Span limitation

$$\tan \beta \leq \frac{B(b+c_r m)-c_r}{Bc_r+b+c_r m}$$

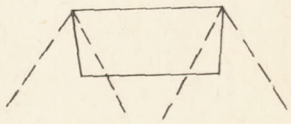
$$C_l = \frac{M_\xi}{qSb} = \frac{M_\xi}{qc_r b(b+c_r m)}$$

$$-m \leq \frac{1}{B+\sqrt{B^2+1}}$$

Phase 1, $0 \leq \tan \beta \leq -m$

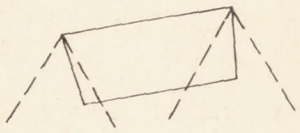


$$M_\xi = M_O + M_S + M_N$$
$$-(b/2)(L_O - L_N)$$



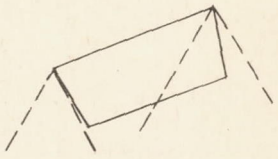
Phase 2, $-m \leq \tan \beta \leq \frac{1+Bm}{B-m}$

$$M_\xi = M_P + M_S + M_N$$
$$-(b/2)(L_P - L_N)$$



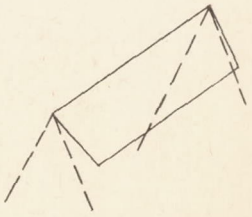
Phase 3, $\frac{1+Bm}{B-m} \leq \tan \beta \leq \frac{1-Bm}{B+m}$

$$M_\xi = M_P + M_T - L_P(b/2)$$



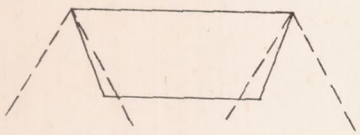
Phase 4, $\frac{1-Bm}{B+m} \leq \tan \beta \leq$ Span limitation

$$M_\xi = M_V + M_Q + M_T$$
$$-(b/2)(L_V + L_Q)$$

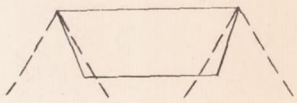


$$-m > \frac{1}{B+\sqrt{B^2+1}}$$

Phase 1, $0 \leq \tan \beta \leq \frac{1+Bm}{B-m}$

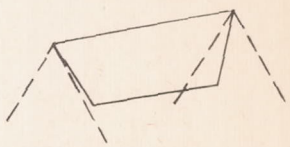


$$M_\xi = M_O + M_S + M_N - (b/2)(L_O - L_N)$$



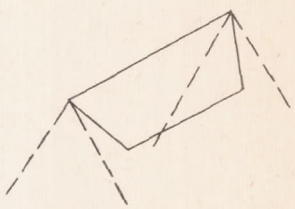
Phase 2, $\frac{1+Bm}{B-m} \leq \tan \beta \leq -m$

$$M_\xi = M_O + M_T - (b/2) L_O$$



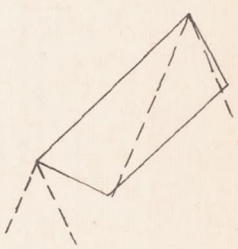
Phase 3, $-m \leq \tan \beta \leq \frac{1-Bm}{B+m}$

$$M_\xi = M_P + M_T - (b/2) L_P$$



Phase 4, $\frac{1-Bm}{B+m} \leq \tan \beta \leq$ Span limitation

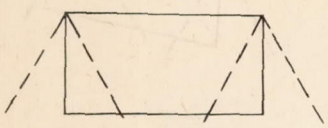
$$M_\xi = M_V + M_Q + M_T - (b/2)(L_V + L_Q)$$



Bm=0 (Rectangular)

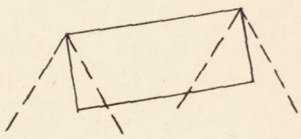
Span limitation

$$\tan \beta \leq \frac{Bb-c_r}{Bc_r+b}$$



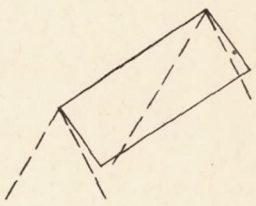
$$C_l = \frac{M_\xi}{qSb} = \frac{M_\xi}{qc_r b^2}$$

Phase 1, $0 \leq \tan \beta \leq 1/B$



$$M_\xi = M_P + M_S + M_N - (L_P - L_N)b/2$$

Phase 2, $1/B \leq \tan \beta \leq$ Span limitation



$$M_\xi = M_V + M_Q + M_T - (L_V + L_Q)b/2$$

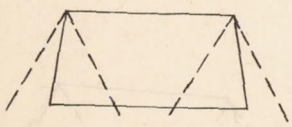
$0 < Bm < 1$

Span limitation

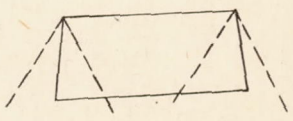
$$\tan \beta \leq \frac{B(b-mc_r)-c_r}{Bc_r+b-mc_r}$$

$$C_l = \frac{M_\xi}{qSb} = \frac{M_\xi}{qc_r b(b-mc_r)}$$

$$m \leq \frac{1}{B+\sqrt{B^2+1}}$$



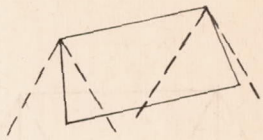
Phase 1, $0 \leq \tan \beta \leq m$



$$M_\xi = M_P + M_R + M_M - \left(\frac{b}{2} - mc_r\right)(L_P - L_M)$$

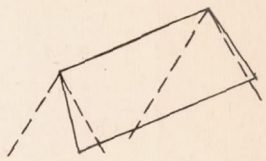
Phase 2, $m \leq \tan \beta \leq \frac{1-Bm}{B+m}$

$$M_\xi = M_P + M_R + M_N - \left(\frac{b}{2} - mc_r\right)(L_P - L_N)$$



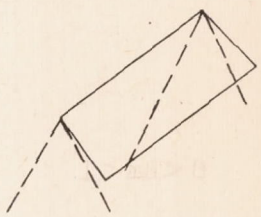
Phase 3, $\frac{1-Bm}{B+m} \leq \tan \beta \leq \frac{1+Bm}{B-m}$

$$M_\xi = M_V + M_Q + M_R + M_N - (L_V + L_Q - L_N)\left(\frac{b}{2} - mc_r\right)$$



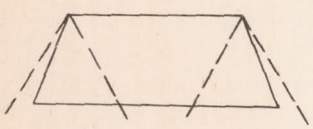
Phase 4, $\frac{1+Bm}{B-m} \leq \tan \beta \leq$ Span limitation

$$M_\xi = M_V + M_Q + M_T - (L_V + L_Q)\left(\frac{b}{2} - mc_r\right)$$

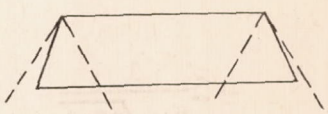


$m > \frac{1}{B + \sqrt{B^2+1}}$

Phase 1, $0 \leq \tan \beta \leq \frac{1-Bm}{B+m}$

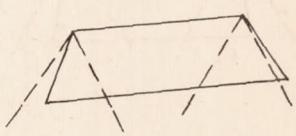


$$M_\xi = M_P + M_R + M_M - (L_P - L_M)\left(\frac{b}{2} - mc_r\right)$$

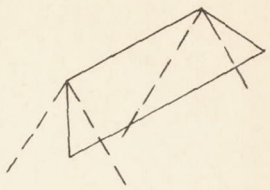


Phase 2, $\frac{1-Bm}{B+m} \leq \tan \beta \leq m$

$$M_\xi = M_V + M_Q + M_R + M_M - (L_V + L_Q - L_M)\left(\frac{b}{2} - mc_r\right)$$

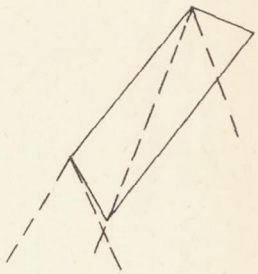


Phase 3, $m \leq \tan \beta \leq \frac{1+Bm}{B-m}$



$$M_\xi = M_V + M_Q + M_R + M_N - (L_V+L_Q-L_N)\left(\frac{b}{2} - mc_r\right)$$

Phase 4, $\frac{1+Bm}{B-m} \leq \tan \beta \leq$ Span limitation



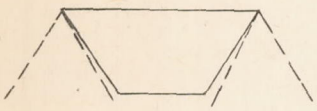
$$M_\xi = M_V + M_Q + M_T - (L_V+L_Q)\left(\frac{b}{2} - mc_r\right)$$

Supersonic Tips

$Bm \leq -1$

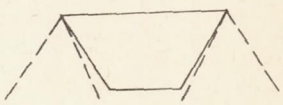
Span limitation

$$\tan \beta \leq \frac{B(mc_r+b)-c_r}{Bc_r+b+mc_r}$$



$$C_l = \frac{M_\xi}{qSb} = \frac{M_\xi}{qc_r b(b+mc_r)}$$

Phase 1, $0 \leq \tan \beta \leq -\left(\frac{Bm+1}{B-m}\right)$



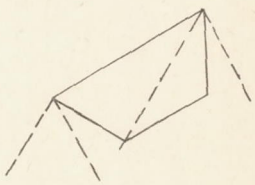
$$M_\xi = 0$$

Phase 2, $-\left(\frac{Bm+1}{B-m}\right) \leq \tan \beta \leq -m$



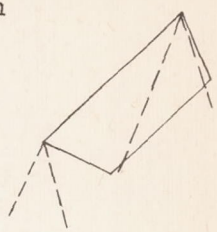
$$M_\xi = M_O + M_T - L_O(b/2)$$

Phase 3, $-m \leq \tan \beta \leq \left(\frac{1-Bm}{B+m}\right)$



$$M_\xi = M_P + M_T - L_P(b/2)$$

Phase 4, $\left(\frac{1-Bm}{B+m}\right) \leq \tan \beta \leq$ Span limitation

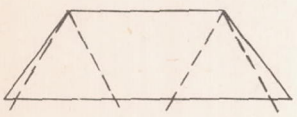


$$M_\xi = M_V + M_Q + M_T - (L_V+L_Q)b/2$$

Span limitation

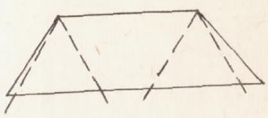
$$\tan \beta \leq \frac{B(b-mc_r)-c_r}{Bc_r+b-mc_r}$$

$Bm \geq 1$



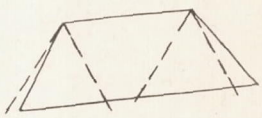
$$C_l = \frac{M_\xi}{qSb} = \frac{M_\xi}{qc_r b(b-mc_r)}$$

Phase 1, $0 \leq \tan \beta \leq \frac{Bm-1}{B+m}$



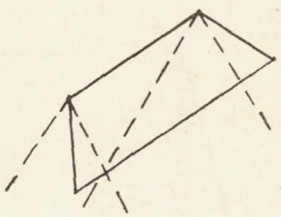
$$M_\xi = M_V + M_Q + M_R + M_L + M_U - (L_V+L_Q-L_L-L_U)\left(\frac{b}{2}-mc_r\right)$$

Phase 2, $\frac{Bm-1}{B+m} \leq \tan \beta \leq m$



$$M_\xi = M_V + M_Q + M_R + M_M - (L_V+L_Q-L_M)\left(\frac{b}{2}-mc_r\right)$$

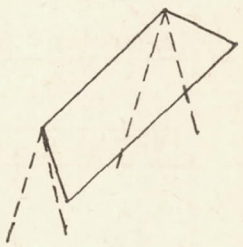
Phase 3, $m \leq \tan \beta \leq \frac{1+Bm}{B-m}$



$$M_\xi = M_V + M_Q + M_R + M_N$$

$$- (L_V+L_Q-L_N)\left(\frac{b}{2} - mc_r\right)$$

Phase 4, $\frac{1+Bm}{B-m} \leq \tan \beta \leq$ Span limitation



$$M_\xi = M_V + M_Q + M_T$$

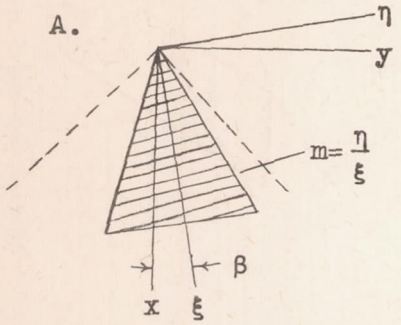
$$-(L_V+L_Q)\left(\frac{b}{2} - mc_r\right)$$

APPENDIX B

SUMMARY OF MOMENT AND ESSENTIAL LIFT EXPRESSIONS

Triangular Wings

A.



$$M_A = \frac{-2\pi\alpha q c_r s m^2 \sin\beta}{3E}\sqrt{\frac{G}{Bm}}$$

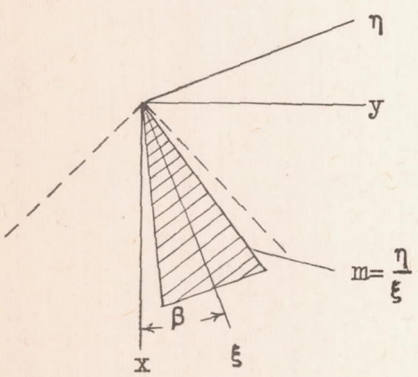
where

E is the complete elliptic integral of the second kind with modulus

$\sqrt{1-G^2}$

$$G = \frac{(1-m^2\tan^2\beta) + B^2(m^2-\tan^2\beta)}{2Bm(1+\tan^2\beta)} - \frac{\sqrt{[(1+m\tan\beta)^2 - B^2(m-\tan\beta)^2][(1-m\tan\beta)^2 - B^2(m+\tan\beta)^2]}}{2Bm(1+\tan^2\beta)}$$

B. $\tan\beta \geq m$



$$M_B = \frac{-2\pi\alpha q c_r^3 m^2 P}{3B}\sqrt{\frac{1-m\tan\beta}{1+m\tan\beta}}$$

when $\tan\beta = m$

$$P = \frac{1}{E}\sqrt{\frac{G_1 Bm}{(1-m^2)}}$$

when $\tan\beta = \frac{1-Bm}{B+m}$

$$P = \frac{\sqrt{2}\sqrt{1+m\tan\beta}}{\pi\sqrt{1+m(\tan\beta)+\beta(m-\tan\beta)}}$$

when $m < \tan\beta < \frac{1-Bm}{B+m}$

$$P = \sqrt{\frac{[B(m+\tan\beta) - G_1(1-m\tan\beta)](1+m\tan\beta)}{[G_1(1+m\tan\beta)+B(m-\tan\beta)](1-m\tan\beta)(1-G_1^2)}} \left\{ \frac{G_1 + k'}{\frac{k'K}{G_1} + E + \frac{k'\sqrt{1-G_1^2}}{\sqrt{G_1^2-k'^2}}[E\,F(\varphi,k) - K\,E(\varphi,k)]} \right\}$$

where

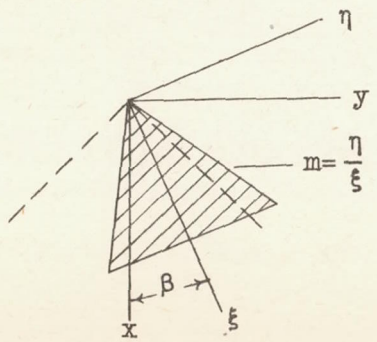
$$G_1 = \frac{(1-m^2\tan^2\beta) - B^2(m^2-\tan^2\beta) - \sqrt{[(1+m\tan\beta)^2 - B^2(m-\tan\beta)^2][(1-m\tan\beta)^2 - B^2(m+\tan\beta)^2]}}{2B\tan\beta\,(1+m^2)}$$

$$k = \sqrt{1-k'^2} \qquad k' = \frac{G_1(1+m\tan\beta)+B(m-\tan\beta)}{(1+m\tan\beta)+G_1B(m-\tan\beta)}$$

$$\varphi = \arcsin\frac{\sqrt{G_1^2-k'^2}}{G_1k}$$

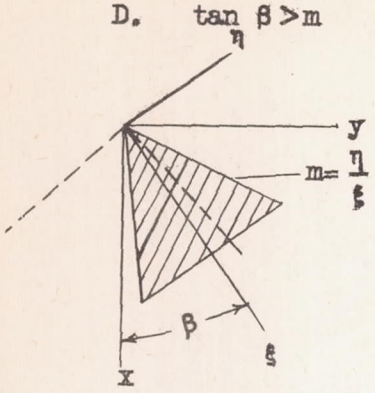
$$K = F\left(\frac{\pi}{2}, k\right)$$

C. $\tan\beta < m$



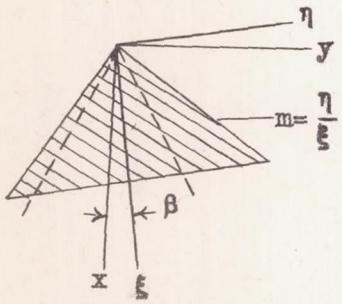
$$M_C = \frac{q\alpha c_r^3\sqrt{2m}\,[2m^2(B+\tan\beta) - 2m(1+B\tan\beta) - 4m\tan^2\beta]}{3(B+\tan\beta)^{3/2}\sqrt{m(B-\tan\beta) + (1+B\tan\beta)}}$$

D. $\tan \beta > m$



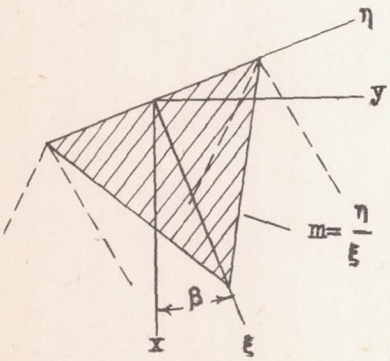
$$M_D = \frac{-q\alpha c_r^3 \sqrt{2m}\,(m+\tan\beta)[m(B+\tan\beta)+(1-B\tan\beta)]}{3(B+\tan\beta)^{3/2}\sqrt{m(B-\tan\beta)+(1+B\tan\beta)}}$$

E.



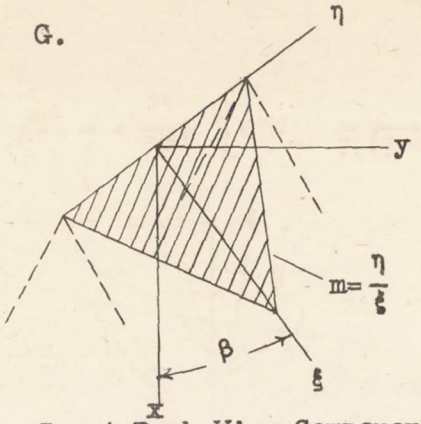
$$M_E = \frac{4q\alpha c_r^3\, m(\tan\beta)(1+\tan^2\beta)}{3(B^2-\tan^2\beta)^{3/2}}$$

F.



$$M_F = \frac{-\alpha q b^3 m\,[1+B(\tan\beta)+m\,(B-\tan\beta)]}{6\sqrt{2}\,\sqrt{B+\tan\beta}\,[m^2(B-\tan\beta)-m(1+B\tan\beta)]^{3/2}}$$

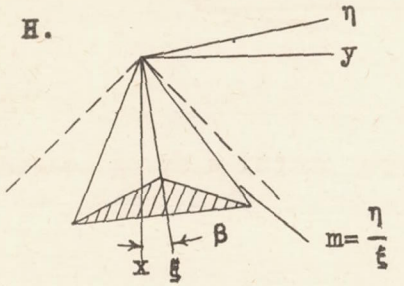
G.



Swept-Back Wing Components

$$M_G = \frac{-\alpha q b^3[11m^2(B-\tan\beta)-11(\tan\beta)(1+B\tan\beta)-9m(1+\tan^2\beta)]}{12\sqrt{2}\sqrt{B+\tan\beta}\,[m^2(B-\tan\beta)-m(1+B\tan\beta)]^{3/2}}$$

H.



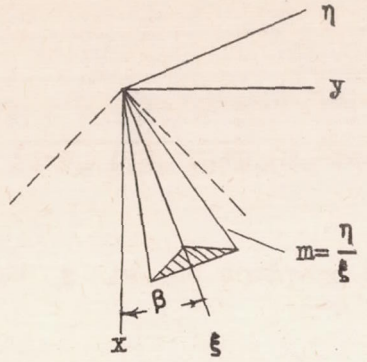
$$M_H = \frac{-4\alpha l^3 m^2 \sin\beta}{3E}\sqrt{\frac{G}{Bm}}\left\{\frac{\pi}{2} - c_r{}^3\left[\frac{3(l-c_r)}{[l^2-(l-c_r)^2]^2}\right.\right.$$

$$\left.\left.+\left(\arcsin\frac{(l-c_r)}{l}+\frac{\pi}{2}\right)\frac{[l^2+2(l-c_r)^2]}{[l^2-(l-c_r)^2]^{5/2}}\right]\right\}$$

where E is the complete elliptic integral of the second kind with modulus $\sqrt{1-G^2}$

$$G = \frac{(1-m^2\tan^2\beta)+B^2(m^2-\tan^2\beta)-\sqrt{[(1+m\tan\beta)^2-B^2(m-\tan\beta)^2][(1-m\tan\beta)^2-B^2(m+\tan\beta)^2]}}{2Bm\,(1+\tan^2\beta)}$$

I.

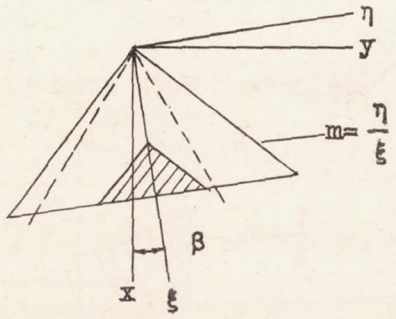


$$M_I = -\frac{4\alpha}{3B} q l^3 m^2 P \sqrt{\frac{1-m\tan\beta}{1+m\tan\beta}}\left(\frac{\pi}{2} - c_r{}^3\left\{\frac{3(l-c_r)}{[l^2-(l-c_r)^2]^2}\right.\right.$$

$$\left.\left. + \left[\arcsin\frac{(l-c_r)}{l} + \frac{\pi}{2}\right]\frac{[l^2+2(l-c_r)^2]}{[l^2-(l-c_r)^2]^{5/2}}\right\}\right)$$

where P is a factor defined under M_B

J.



$$m > \left(\frac{1+B\tan\beta}{B-\tan\beta}\right)$$

$$M_J = M_{J_1} + M_{J_2}$$

$$M_{J_1} = +\frac{4\alpha q}{3\pi}\left[\sin^{-1}\frac{l[(1-m\tan\beta)-B^2(\tan\beta)(m+\tan\beta)]+m(l-c_r)[(\tan\beta)(1-m\tan\beta)+B^2(m+\tan\beta)]}{mB(1+\tan^2\beta)(2l-c_r)}\right.$$

$$\left\{\frac{(m+\tan\beta)}{\sqrt{B^2(m+\tan\beta)^2-(1-m\tan\beta)^2}}\right\}\left\{-\frac{3m^2lc_r(l-c_r)}{2}-\frac{3c_r{}^3m^2}{8}\right\}$$

$$+\sin^{-1}\frac{(1-m\tan\beta)-B^2(\tan\beta)(m+\tan\beta)}{mB(1+\tan^2\beta)}\left\{\frac{-c_r{}^3m^3}{\sqrt{B^2(m+\tan\beta)^2-(1-m\tan\beta)^2}}\right\}$$

$$\left\{(m+\tan\beta)\left(-\frac{3}{8m}+\frac{(\tan\beta)(1-m\tan\beta)+B^2(m+\tan\beta)}{B^2(m+\tan\beta)^2-(1-m\tan\beta)^2}\right.\right.$$

$$\left.-\frac{3m[(\tan\beta)(1-m\tan\beta)+B^2(m+\tan\beta)]^2}{4[B^2(m+\tan\beta)^2-(1-m\tan\beta)^2]^2}+\frac{m(B^2-\tan^2\beta)}{4[B^2(m+\tan\beta)^2-(1-m\tan\beta)^2]}\right)$$

$$\left.+(m-\tan\beta)\left(-\frac{3}{8m}+\frac{(\tan\beta)(1-m\tan\beta)+B^2(m+\tan\beta)}{4[B^2(m+\tan\beta)^2-(1-m\tan\beta)^2]}\right)\right\}$$

$$+\sqrt{(1-B^2\tan^2\beta)l^2+2(\tan\beta)(B^2+1)ml(l-c_r)-(B^2-\tan^2\beta)m^2(l-c_r)^2}$$

$$\left\{(m+\tan\beta)\left(\frac{l^2}{2(B^2-\tan^2\beta)}-\frac{c_r{}^2m^2}{4[B^2(m-\tan\beta)^2-(1+m\tan\beta)^2]}\right)\right.$$

$$+\ (m-\tan\beta)\left(\frac{l^2}{2(B^2-\tan^2\beta)}-\frac{c_r{}^2m^2}{B^2(m-\tan\beta)^2-(1+m\tan\beta)^2}+\frac{lc_rm^2}{4[B^2(m-\tan\beta)^2-(1+m\tan\beta)^2]}\right.$$

$$\left.\left.-\frac{3c_r{}^2m^3[(\tan\beta)(1+m\tan\beta)-B^2(m-\tan\beta)]}{4[B^2(m-\tan\beta)^2-(1+m\tan\beta)^2]^2}\right)\right\}$$

$$+\ \sqrt{1-B^2\tan^2\beta}\left\{-c_r{}^3m^3\right\}\left\{(m+\tan\beta)\left(\frac{3}{4m[B^2(m+\tan\beta)^2-(1-m\tan\beta)^2]}\right.\right.$$

$$\left.\left.-\frac{3[(\tan\beta)(1-m\tan\beta)+B^2(m+\tan\beta)]}{4[B^2(m+\tan\beta)^2-(1-m\tan\beta)^2]^2}-\frac{1}{4m[B^2(m-\tan\beta)^2-(1+m\tan\beta)^2]}\right)\right.$$

$$+\ (m-\tan\beta)\left(\frac{1}{4m[B^2(m+\tan\beta)^2-(1-m\tan\beta)^2]}-\frac{3}{4m[B^2(m-\tan\beta)^2-(1+m\tan\beta)^2]}\right.$$

$$- \frac{3[(\tan\beta)(1+m\tan\beta)-B^2(m-\tan\beta)]}{4[B^2(m-\tan\beta)^2-(1+m\tan\beta)^2]^2}\Bigg)\Bigg\}$$

$$+ \sin^{-1}\frac{l[(1+m\tan\beta)+B^2(\tan\beta)(m-\tan\beta)]+m(l-c_r)[(\tan\beta)(1+m\tan\beta)-B^2(m-\tan\beta)]}{mB(1+\tan^2\beta)c_r}$$

$$\left\{\frac{(m+\tan\beta)}{\sqrt{B^2(m-\tan\beta)^2-(1+m\tan\beta)^2}}\left(\frac{3c_r{}^3m^2}{8}+\frac{c_r{}^3m^3[(\tan\beta)(1+m\tan\beta)-B^2(m-\tan\beta)]}{4[B^2(m-\tan\beta)^2-(1+m\tan\beta)^2]}\right)\right.$$

$$+\frac{(m-\tan\beta)}{\sqrt{B^2(m-\tan\beta)^2-(1+m\tan\beta)^2}}\left(-\frac{3lc_rm^2(l-c_r)}{2}-\frac{c_r{}^3m^4(B^2-\tan^2\beta)}{4[B^2(m-\tan\beta)^2-(1+m\tan\beta)^2]}\right.$$

$$\left.\left.+\frac{c_r{}^3m^3[(\tan\beta)(1+m\tan\beta)-B^2(m-\tan\beta)]}{B^2(m-\tan\beta)^2-(1+m\tan\beta)^2}+\frac{3c_r{}^3m^4[(\tan\beta)(1+m\tan\beta)-B^2(m-\tan\beta)]^2}{4[B^2(m-\tan\beta)^2-(1+m\tan\beta)^2]^2}\right)\right\}$$

$$+ \sin^{-1} \frac{(1+m \tan \beta)+B^2(\tan \beta)(m-\tan \beta)}{m B(1+\tan^2 \beta)} \left\{ \frac{(m+\tan \beta)}{\sqrt{B^2(m-\tan \beta)^2-(1+m \tan \beta)^2}} \left(- \frac{3c_r{}^3m^2}{8} \right. \right.$$

$$- \frac{c_r{}^3m^3[(\tan \beta)(1+m \tan \beta)-B^2(m-\tan \beta)]}{4[B^2(m-\tan \beta)^2-(1+m \tan \beta)^2]} \Bigg) + \frac{(m-\tan \beta)}{\sqrt{B^2(m-\tan \beta)^2-(1+m \tan \beta)^2}} \left(- \frac{3c_r{}^3m^2}{8} \right.$$

$$- \frac{c_r{}^3m^3[(\tan \beta)(1+m \tan \beta)-B^2(m-\tan \beta)]}{B^2(m-\tan \beta)^2-(1+m \tan \beta)^2} - \frac{3c_r{}^3m^4[(\tan \beta)(1+m \tan \beta)-B^2(m-\tan \beta)]^2}{4[B^2(m-\tan \beta)^2-(1+m \tan \beta)^2]^2}$$

$$\left. \left. + \frac{c_r{}^3m^4(B^2-\tan^2 \beta)}{4[B^2(m-\tan \beta)^2-(1+m \tan \beta)^2]} \right) \right\}$$

$$+ \sin^{-1} \frac{(\tan \beta)(B^2+1)l-(B^2-\tan^2 \beta)m(l-c_r)}{Bl(1+\tan^2 \beta)} \left\{ \frac{l^3m(\tan \beta)(1+\tan^2 \beta)}{(B^2-\tan^2 \beta)^{3/2}} \right\} \Bigg]$$

$$M_{J_2} = + \frac{4\alpha q}{3\pi} \left[- \sin^{-1} \frac{l(\tan\beta)(B^2+1)+m(l-c_r)(B^2-\tan^2\beta)}{Bl(1+\tan^2\beta)} \left\{ \frac{l^3 m(\tan\beta)(1+\tan^2\beta)}{(B^2-\tan^2\beta)^{3/2}} \right\} \right.$$

$$- \sin^{-1} \frac{[(1-m\tan\beta)-B^2(\tan\beta)(m+\tan\beta)]l-[(\tan\beta)(1-m\tan\beta)+B^2(m+\tan\beta)]m(l-c_r)}{mB(1+\tan^2\beta)\,c_r}$$

$$\left\{ \frac{m+\tan\beta}{\sqrt{B^2(m+\tan\beta)^2-(1-m\tan\beta)^2}} \left(- \frac{3lc_r m^2(l-c_r)}{2} - \frac{c_r^3 m^3[(\tan\beta)(1-m\tan\beta)+B^2(m+\tan\beta)]}{B^2(m+\tan\beta)^2-(1-m\tan\beta)^2} \right. \right.$$

$$\left. + \frac{3c_r^3 m^4[(\tan\beta)(1-m\tan\beta)+B^2(m+\tan\beta)]^2}{4[B^2(m+\tan\beta)^2-(1-m\tan\beta)]^2} - \frac{c_r^3 m^4(B^2-\tan^2\beta)}{4[B^2(m+\tan\beta)^2-(1-m\tan\beta)^2]} \right)$$

$$\left. - \frac{(m-\tan\beta)}{\sqrt{B^2(m+\tan\beta)^2-(1-m\tan\beta)^2}} \left(\frac{c_r^3 m^3[(\tan\beta)(1-m\tan\beta)+B^2(m+\tan\beta)]}{4[B^2(m+\tan\beta)^2-(1-m\tan\beta)^2]} - \frac{3c_r^3 m^2}{8} \right) \right\}$$

$$- \sqrt{(1-B^2\tan^2\beta)l^2-2(\tan\beta)(B^2+1)ml(l-c_r)-(B^2-\tan^2\beta)m^2(l-c_r)^2}$$

$$\left\{(m+\tan\beta)\left(\frac{l^2}{2(B^2-\tan^2\beta)}-\frac{c_r^2m^2}{[B^2(m+\tan\beta)^2-(1-m\tan\beta)^2]}\right.\right.$$

$$+\frac{lc_rm^2}{4[B^2(m+\tan\beta)^2-(1-m\tan\beta)^2]}+\left.\frac{3c_r^2m^3[(\tan\beta)(1-m\tan\beta)+B^2(m+\tan\beta)]}{4[B^2(m+\tan\beta)^2-(1-m\tan\beta)^2]}\right)$$

$$\left.+(m-\tan\beta)\left(\frac{l^2}{2(B^2-\tan^2\beta)}-\frac{c_r^2m^2}{4[B^2(m+\tan\beta)^2-(1-m\tan\beta)^2]}\right)\right\}$$

$$-\sin^{-1}\frac{[(1+m\tan\beta)+B^2(\tan\beta)(m-\tan\beta)]l-[(\tan\beta)(1+m\tan\beta)-B^2(m-\tan\beta)]m(l-c_r)}{mB(1+\tan^2\beta)(2l-c_r)}$$

$$\left.\left\{\frac{(m-\tan\beta)}{\sqrt{B^2(m-\tan\beta)^2-(1+m\tan\beta)^2}}\left(\frac{3lc_rm^2(l-c_r)}{2}-\frac{3c_r^3m^2}{8}\right)\right\}\right]$$

$$m = \left(\frac{1+B\tan\beta}{B-\tan\beta}\right)^{a}$$

$$M_{J_1} = +\frac{4\alpha q}{3\pi}\left[\sin^{-1}\frac{2B(m^2+1)l-[2m(B^2-1)+B(3m^2-1)]c_r}{B(m^2+1)(2l-c_r)}\right.$$

$$\left\{\frac{m^2+2Bm-1}{2\sqrt{m(1+B^2)(mB-1)(m+B)}}\right\}\left\{-\frac{3lc_rm^2(l-c_r)}{2}-\frac{3c_r^3m^2}{8}\right\}$$

$$+\sqrt{m(B^2+1)[2B(m^2+1)lc_r-m(B^2+2Bm-1)c_r^2]}\left\{\left(\frac{(m^2+2Bm-1)}{1+B^2}\right)\right.$$

$$\left(\frac{l^2}{2(B^2+2Bm-1)}+\frac{lc_rm}{12B(1+m^2)}+\frac{c_r^2m^2(B^2+2Bm-1)}{12B^2(1+m^2)^2}\right.$$

$$\left.-\frac{3c_r^2m}{8B(1+m^2)}\right)+\frac{1}{B(1+B^2)}\left(\frac{l^2(m+2B-B^2m)}{(B^2+2Bm-1)}+\frac{lm(l-c_r)}{2}\right.$$

$$+\frac{3l^2(mB-1)(m+B)}{2(B^2+2Bm-1)}-\frac{lc_rm[2B(2m^2+1)+m(B^2-1)]}{3B(m^2+1)}$$

$$\left.+\frac{2l^2m}{5}\right)+\frac{B^2+2Bm-1}{B^2(1+m^2)(1+B^2)}\left(c_r^2m^2-\frac{c_r^2m^2[2B(2m^2+1)+m(B^2-1)]}{3B(1+m^2)}\right.$$

[a]Left leading edge hits Mach cone from apex.

$$+\frac{4lc_rm^2}{15}+\frac{4c_r^2m^3(B^2+2Bm-1)}{15B(m^2+1)}\Bigg)\Bigg\}$$

$$+\sin^{-1}\frac{c_rm(B^2+2Bm-1)-Bl(m^2+1)}{Bl(m^2+1)}\left\{\frac{l^3m(1+m^2)(Bm-1)}{(B^2+2Bm-1)^{3/2}\sqrt{1+B^2}}\right\}$$

$$+\sin^{-1}\frac{2m(1-B^2)+B(3-m^2)}{B(1+m^2)}\left\{\frac{c_r^3m^2}{2\sqrt{m(1+B^2)(mB-1)(m+B)}}\right\}$$

$$\left\{(m^2+2Bm-1)\left(\frac{3}{8}-\frac{[2m(B^2-1)+B(3m^2-1)]}{4(m+B)(mB-1)}\right.\right.$$

$$+\frac{3[2m(B^2-1)+B(3m^2-1)]^2}{64(m+B)^2(mB-1)^2}-\frac{m(B^2+2Bm-1)}{16(m+B)(mB-1)}\Bigg)$$

$$+\frac{3m(B^2+2Bm-1)}{4B}-\frac{[B(3m^2-1)+2m(B^2-1)][2B(2m^2-1)+3m(B^2-1)]}{4B(m+B)(mB-1)}$$

$$\left.+\frac{3[B(3m^2-1)+2m(B^2-1)]^2}{16B(m+B)(mB-1)}\Bigg)\right\}$$

$$+\sqrt{m(1+B^2)(m+2B-B^2m)}\left\{\frac{c_r^3m}{(m+B)}\right\}\left\{\frac{(m^2+2mB-1)}{(m+B)(1+B^2)}\left(-\frac{3(m+B)}{16(mB-1)}\right.\right.$$

$$+\frac{3[2m(B^2-1)+B(3m^2-1)]}{64(mB-1)^2}-\frac{(m+B)^2}{12B(1+m^2)}-\frac{m(B^2+2Bm-1)(m+B)^2}{12B^2(1+m^2)^2}$$

$$+\frac{3(m+B)^2}{8B(1+m^2)}\Bigg)+\frac{1}{B(1+B^2)}\Bigg(-\frac{[2B(2m^2-1)+3m(B^2-1)]}{4(mB-1)}+\frac{m+B}{4}$$

$$+\frac{3[B(3m^2-1)+2m(B^2-1)]}{16(mB-1)}-\frac{m(B^2+2Bm-1)(m+B)}{B(m^2+1)}$$

$$+\frac{(m+B)[2B(2m^2+1)+3m(B^2-1)]}{3B(m^2+1)}+\frac{m(B^2+2Bm-1)[2B(2m^2+1)+3m(B^2-1)](m+B)}{3B^2(m^2+1)^2}$$

$$-\frac{2(m+B)}{5}-\frac{4m(B^2+2Bm-1)(m+B)}{15B(m^2+1)}-\frac{4m^2(B^2+2Bm-1)^2(m+B)}{15B^2(m^2+1)^2}\Bigg)\Bigg\}\Bigg]$$

$$M_{J_2}=+\frac{4\alpha q}{3\pi}\Bigg[\sin^{-1}\frac{4l(mB-1)(m+B)-[2m(B^2-1)+B(3m^2-1)]c_r}{B(1+m^2)c_r}$$

$$\Bigg\{\frac{m^2+2mB-1}{2\sqrt{m(1+B^2)(mB-1)(m+B)}}\Bigg\}\Bigg\{\frac{3lc_rm^2(l-c_r)}{2}+\Bigg(\frac{c_r^3m^2}{4(mB-1)(m+B)}\Bigg)$$

$$\Bigg(2m(B^2-1)+B(3m^2-1)-\frac{3[2m(B^2-1)+B(3m^2-1)]^2}{16(m+B)(mB-1)}+\frac{m(B^2+2mB-1)}{4}\Bigg)\Bigg\}$$

$$+\sqrt{m(1+B^2)\left[-4l^2(mB-1)(m+B)+2lc_r\left\{2m(B^2-1)+B(3m^2-1)\right\}-c_r{}^2m(B^2+2Bm-1)\right]}$$

$$\left\{-\frac{(m^2+2mB-1)}{(m+B)(1+B^2)}\left(\frac{l^2(m+B)}{2(B^2+2Bm-1)}-\frac{c_r{}^2m}{4(mB-1)}+\frac{lc_rm}{16(mB-1)}\right.\right.$$

$$\left.+\frac{3c_r{}^2m\left[2m(B^2-1)+B(3m^2-1)\right]}{64(m+B)(mB-1)^2}\right)+\left(\frac{1}{B(m+B)(1+B^2)}\right)$$

$$\left(-\frac{l^2(m+2B-B^2m)(m+B)}{(B^2+2Bm-1)}+\frac{lm(l-c_r)(m+B)}{2}\right.$$

$$-\frac{3l^2(mB-1)(m+B)^2}{2(B^2+2Bm-1)}+\frac{c_r{}^2m\left[2B(2m^2-1)+3m(B^2-1)\right]}{4(mB-1)}$$

$$\left.\left.-\frac{lc_rm(m+B)}{4}-\frac{3c_r{}^2m\left[B(3m^2-1)+2m(B^2-1)\right]}{16(mB-1)}\right)\right\}$$

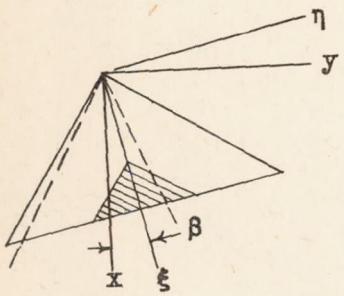
$$-\sin^{-1}\frac{l\left[B(3m^2-1)+2m(B^2-1)\right]-c_rm(B^2+2Bm-1)}{Bl(m^2+1)}\left\{\frac{l^3m(1+m^2)(mB-1)}{(B^2+2Bm-1)^{3/2}\sqrt{1+B^2}}\right\}$$

$$+ \sin^{-1} \frac{4l(mB-1)(B+m)-[2m(B^2-1)+B(3m^2-1)]c_r}{B(1+m^2)c_r} \left\{ - \frac{c_r{}^3 m^2}{8B\sqrt{m(1+B^2)(mB-1)(m+B)}} \right\}$$

$$\left\{ - 3m(B^2+2Bm-1) + \frac{[2B(2m^2-1)+3m(B^2-1)]\,[B(3m^2-1)+2m(B^2-1)]}{(m+B)(mB-1)} \right.$$

$$\left. - \frac{3[B(3m^2-1)+2m(B^2-1)]^2}{4(m+B)(mB-1)} \right\} \Bigg]$$

K.



$$m > \left(\frac{1+B \tan \beta}{B - \tan \beta} \right)$$

$$M_K = M_{J_1} + M_{K_1}$$

$$M_{K_1} = + \frac{2\alpha q}{3} \left[- \frac{l^3 m \,(\tan \beta)(1 + \tan^2 \beta)}{(B^2 - \tan^2 \beta)^{3/2}} \right.$$

$$+ \frac{(m + \tan \beta)}{\sqrt{B^2(m + \tan \beta)^2 - (1 - m \tan \beta)^2}} \left\{ - \frac{c_r{}^3 m^3 [(\tan \beta)(1 - m \tan \beta) + B^2(m + \tan \beta)]}{B^2(m + \tan \beta)^2 - (1 - m \tan \beta)^2} \right.$$

$$\left. - \frac{c_r{}^3 m^4 (B^2 - \tan^2 \beta)}{4[B^2(m + \tan \beta)^2 - (1 - m \tan \beta)^2]} + \frac{3 c_r{}^3 m^4 [(\tan \beta)(1 - m \tan \beta) + B^2(m + \tan \beta)]^2}{4[B^2(m + \tan \beta)^2 - (1 - m \tan \beta)^2]^2} \right.$$

$$- \frac{3lc_r m^2(l-c_r)}{2} \Bigg\}$$

$$+ \frac{(m-\tan\beta)}{\sqrt{B^2(m-\tan\beta)^2-(1+m\tan\beta)^2}} \left\{ \frac{3c_r{}^3m^2}{8} + \frac{3lc_r m^2(l-c_r)}{2} \right\}$$

$$- \frac{(m-\tan\beta)}{\sqrt{B^2(m+\tan\beta)^2-(1-m\tan\beta)^2}} \left\{ \frac{c_r{}^3m^3[(\tan\beta)(1-m\tan\beta)+B^2(m+\tan\beta)]}{4[B^2(m+\tan\beta)^2-(1-m\tan\beta)^2]} \right.$$

$$\left. - \frac{3c_r{}^3m^2}{8} \right\} \Bigg]$$

$$m = \left(\frac{1+B\tan\beta}{B-\tan\beta} \right)^b$$

$$M_{K_1} = + \frac{2\alpha q}{3} \left[\frac{m^2 + 2Bm - 1}{2\sqrt{m(1+B^2)(mB-1)(m+B)}} \left\{ - \frac{3lc_r m^2(l-c_r)}{2} \right.\right.$$

$$\left. - \frac{c_r{}^3m^2}{4(mB-1)(m+B)} \left(2m(B^2-1)+B(3m^2-1) - \frac{3[2m(B^2-1)+B(3m^2-1)]^2}{16(m+B)(mB-1)} \right.\right.$$

---

[b] Left leading edge hits Mach cone from apex.

$$+\frac{m(B^2+2mB-1)}{4}\Bigg)\Bigg\}-\frac{l^3m(mB-1)(1+m^2)}{(B^2+2Bm-1)^{3/2}\sqrt{1+B^2}}$$

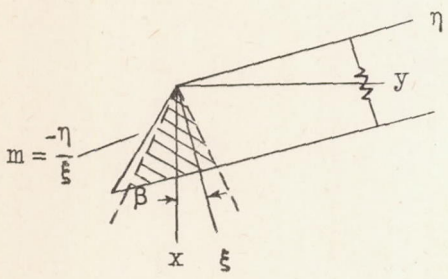
$$-\frac{c_r{}^3m^2}{8B\sqrt{m(1+B^2)(mB-1)(m+B)}}\Big\{-3m(B^2+2Bm-1)$$

$$+\frac{[2B(2m^2-1)+3m(B^2-1)]\,[B(3m^2-1)+2m(B^2-1)]}{(m+B)(mB-1)}$$

$$-\frac{3[B(3m^2-1)+2m(B^2-1)]^2}{4(m+B)(mB-1)}\Big\}\Big]$$

Trapezoidal Wing Components

L_L

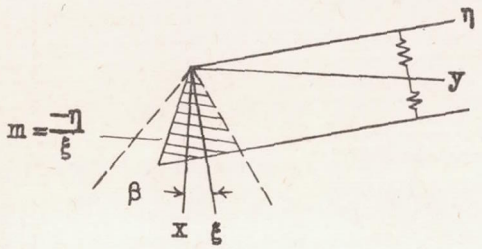


$$L_L=\frac{2q\alpha c_r{}^2[B(1+\tan^2\beta)+(B^2-\tan^2\beta)(m-\tan\beta)]}{(B^2-\tan^2\beta)^{3/2}}$$

$$-\frac{2q\alpha c_r{}^2\,(m-\tan\beta)}{\sqrt{B^2\,(m-\tan\beta)^2-(1+m\tan\beta)^2}}\left[m-\frac{(1+B\tan\beta)}{(B-\tan\beta)}\right]$$

$$M_L = \frac{2q\alpha c_r{}^3(m-\tan\beta)}{3\sqrt{B^2-\tan^2\beta}} \left\{ \frac{(B^2+1)\tan\beta}{(B^2-\tan^2\beta)} + m - \frac{B(1+\tan^2\beta)[-4(\tan\beta)(B^2+1)+B(1+\tan^2\beta)]}{2(B^2-\tan^2\beta)^2(m-\tan\beta)} \right\}$$

M.

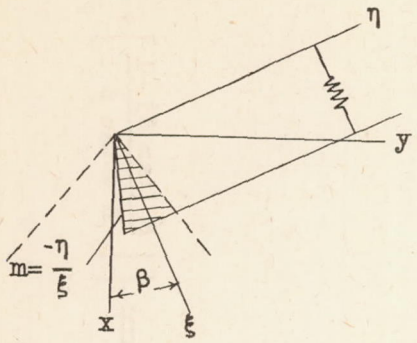


$$L_M = \frac{q\alpha c_r{}^2[3m(B+\tan\beta)+(1-3B\tan\beta-2\tan^2\beta)]}{(B+\tan\beta)\sqrt{B^2-\tan^2\beta}}$$

$$M_M = \frac{q\alpha c_r{}^3}{12(B+\tan\beta)^2\sqrt{B^2-\tan^2\beta}} \left\{ 4[(B+\tan\beta)(m-\tan\beta)][3m(B+\tan\beta)-(1-B\tan\beta)] \right.$$

$$\left. + [3m(B+\tan\beta)-5(1-B\tan\beta)][m(B+\tan\beta)+(1-B\tan\beta)] \right\}$$

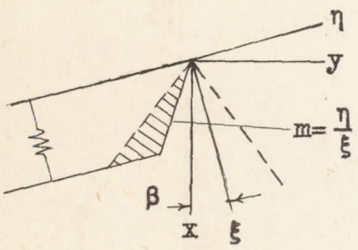
N.



$$L_N = \frac{q\alpha c_r^2[B(m-\tan\beta)+(1+m\tan\beta)]}{(B+\tan\beta)\sqrt{B^2-\tan^2\beta}}$$

$$M_N = \frac{q\alpha c_r^3[3m(B+\tan\beta)-5(1-B\tan\beta)][m(B+\tan\beta)+(1-B\tan\beta)]}{12(B+\tan\beta)^2\sqrt{B^2-\tan^2\beta}}$$

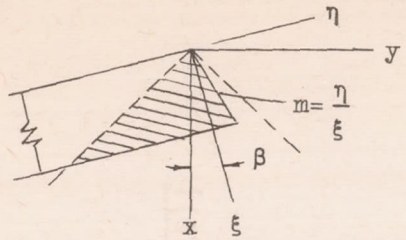
O.



$$L_O = \frac{q\alpha c_r^2[B(m+\tan\beta)+(1-m\tan\beta)]}{(B-\tan\beta)\sqrt{B^2-\tan^2\beta}}$$

$$M_O = \frac{-q\alpha c_r^3[3m(B-\tan\beta)-5(1+B\tan\beta)][m(B-\tan\beta)+(1+B\tan\beta)]}{12(B-\tan\beta)^2\sqrt{B^2-\tan^2\beta}}$$

P.

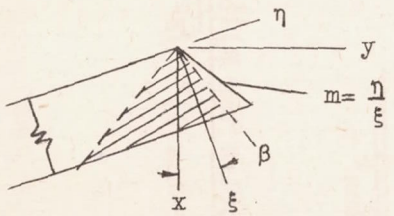


$$L_P = \frac{q\alpha c_r^2[\,3m(B-\tan\beta)+(1+3\,B\tan\beta-2\tan^2\beta)]}{(B-\tan\beta)\sqrt{B^2-\tan^2\beta}}$$

$$M_P = \frac{-q\alpha c_r^3}{12(B-\tan\beta)^2\sqrt{B^2-\tan^2\beta}}\left\{4\,[(B-\tan\beta)(m+\tan\beta)][\,3m(B-\tan\beta)-(1+B\tan\beta)]\right.$$

$$\left.+\,[\,3m(B-\tan\beta)-5(1+B\tan\beta)][\,m(B-\tan\beta)+(1+B\tan\beta)]\right\}$$

Q.

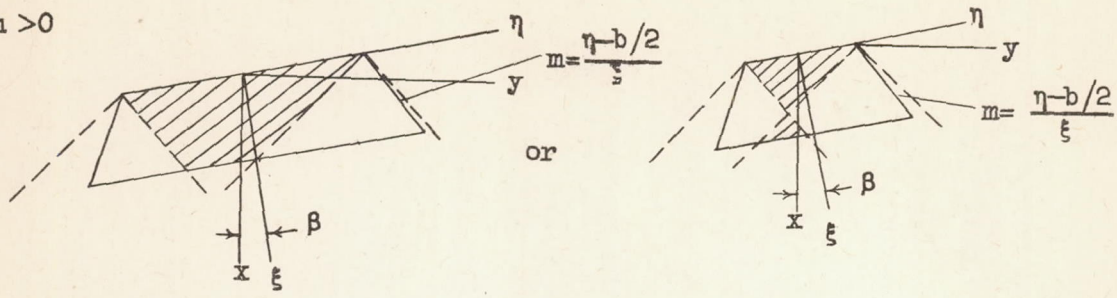


$$L_Q = \frac{2q\alpha c_r^2[B(1+\tan^2\beta)+(B^2-\tan^2\beta)(m+\tan\beta)]}{(B^2-\tan^2\beta)^{3/2}} - \frac{2q\alpha c_r^2\,(m+\tan\beta)}{\sqrt{B^2\,(m+\tan\beta)^2-(1-m\tan\beta)^2}}\left\{\left[\frac{B\,(\tan\beta)-1}{B+\tan\beta}\right]+m\right\}$$

$$M_Q = \frac{2q\alpha c_r^3(m+\tan\beta)}{3\sqrt{B^2-\tan^2\beta}}\left\{\frac{(B^2+1)\tan\beta}{(B^2-\tan^2\beta)}-m\right.$$

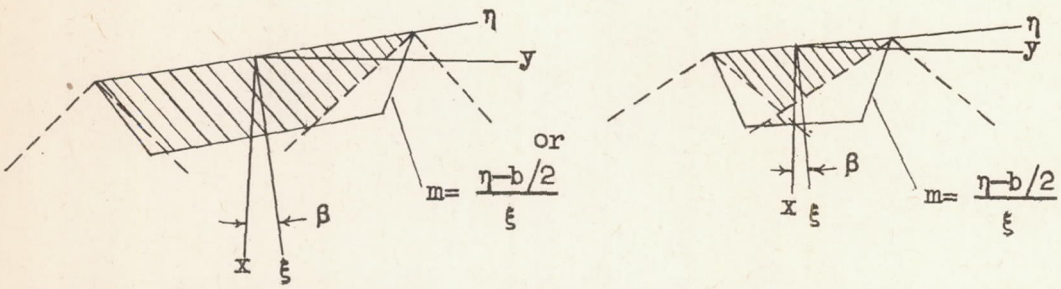
$$\left.+\,\frac{B(1+\tan^2\beta)[\,4(\tan\beta)(B^2+1)+B(1+\tan^2\beta)]}{2(B^2-\tan^2\beta)^2(m+\tan\beta)}\right\}$$

R. $m > 0$



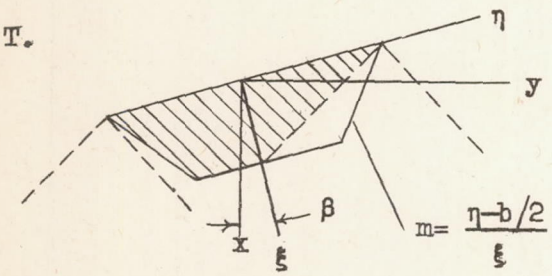
$$M_R = \frac{4\alpha q c_r^2(1+B^2)\tan\beta}{(B^2-\tan^2\beta)^{3/2}}\left[\frac{(b-2c_r m)}{2} - \frac{2c_r B(1+\tan^2\beta)}{3(B^2-\tan^2\beta)}\right]$$

S. $m < 0$



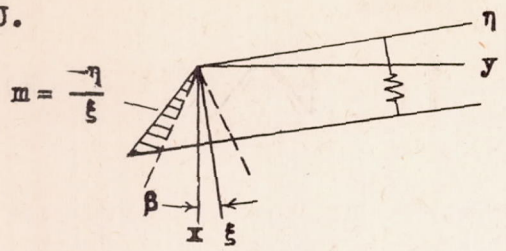
$$M_S = \frac{4\alpha q c_r^2(1+B^2)\tan\beta}{(B^2-\tan^2\beta)^{3/2}}\left[\frac{b}{2} - \frac{2c_r B(1+\tan^2\beta)}{3(B^2-\tan^2\beta)}\right]$$

T.



$$M_T = \frac{2\alpha q c_r^2}{\sqrt{B^2-\tan^2\beta}}\left[\frac{c_r}{3}\left\{m^2 - \left(\frac{1+B\tan\beta}{B-\tan\beta}\right)^2\right\} + \frac{b}{2}\left\{\left(\frac{1+B\tan\beta}{B-\tan\beta}\right) + m\right\}\right]$$

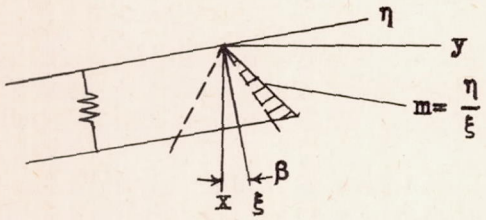
U.



$$L_U = \frac{2q\alpha c_r^2(m-\tan\beta)}{\sqrt{B^2(m-\tan\beta)^2-(1+m\tan\beta)^2}}\left[m-\frac{(1+B\tan\beta)}{(B-\tan\beta)}\right]$$

$$M_U = \frac{2q\alpha c_r^3(m-\tan\beta)}{3\sqrt{B^2(m-\tan\beta)^2-(1+m\tan\beta)^2}}\left[m^2-\left(\frac{1+B\tan\beta}{B-\tan\beta}\right)^2\right]$$

V.



$$L_V = \frac{2\alpha q c_r^2(m+\tan\beta)}{\sqrt{B^2(m+\tan\beta)^2-(1-m\tan\beta)^2}}\left[\left(\frac{B(\tan\beta)-1}{B+\tan\beta}\right)+m\right]$$

$$M_V = \frac{2\alpha q c_r^3(m+\tan\beta)}{3\sqrt{B^2(m+\tan\beta)^2-(1-m\tan\beta)^2}}\left[\left(\frac{B(\tan\beta)-1}{B+\tan\beta}\right)^2-m^2\right]$$

REFERENCES

1. Jones, Arthur L., and Alksne, Alberta: The Damping Due to Roll of Triangular, Trapezoidal, and Related Plan Forms in Supersonic Flow. NACA TN No. 1548, 1948.

2. Heaslet, Max. A., and Lomax, Harvard: The Use of Source-Sink and Doublet Distributions Extended to the Solution of Arbitrary Boundary Value Problems in Supersonic Flow. NACA TN No. 1515, 1948.

3. Evvard, John C.: Distribution of Wave Drag and Lift in the Vicinity of Wing Tips at Supersonic Speeds. NACA TN No. 1382, 1947.

4. Evvard, John C.: Theoretical Distribution of Lift on Thin Wings at Supersonic Speeds (an Extension). NACA TN No. 1585, 1948.

5. Moeckel, W. E.: Effect of Yaw at Supersonic Speeds on Theoretical Aerodynamic Coefficients of Thin Pointed Wings with Several Types of Trailing Edge. NACA TN No. 1549, 1948.

6. Hayes, W. D., Browne, S. H., and Lew, R. J.: Linearized Theory of Conical Supersonic Flow with Application to Triangular Wings. Report No. NA-46-818, North American Aviation, Inc., June 26, 1947.

7. Ribner, Herbert S., and Malvestuto, Frank S., Jr.: Stability Derivatives of Triangular Wings at Supersonic Speeds. NACA TN No. 1572, 1948.

8. Heaslet, Max. A., Lomax, Harvard, and Jones, Arthur L.: Volterra's Solution of the Wave Equation as Applied to Three-Dimensional Supersonic Airfoil Problems. NACA TN No. 1412, 1947.

9. Ribner, Herbert S.: The Stability Derivatives of Low-Aspect-Ratio Triangular Wings at Subsonic and Supersonic Speeds. NACA TN No. 1423, 1947.

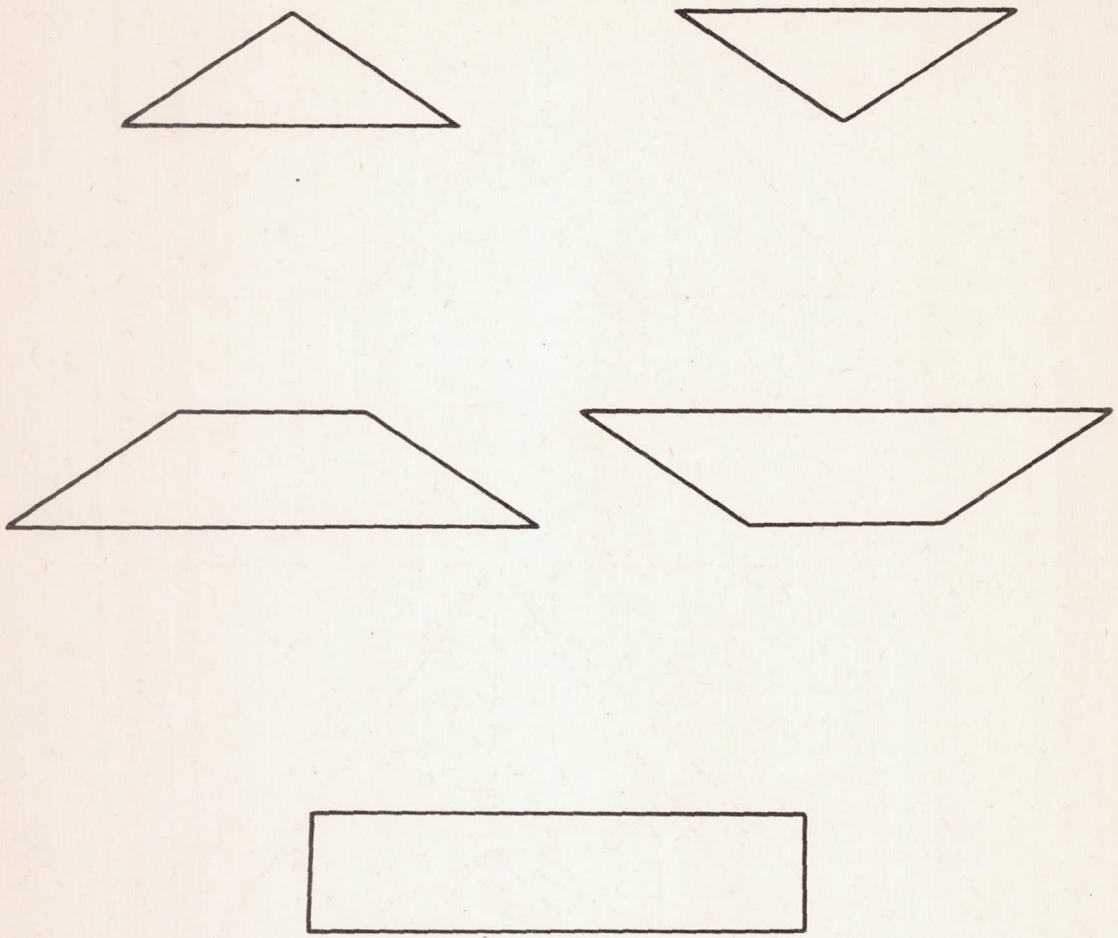


Figure 1.–The triangular, trapezoidal, and rectangular plan form types investigated.

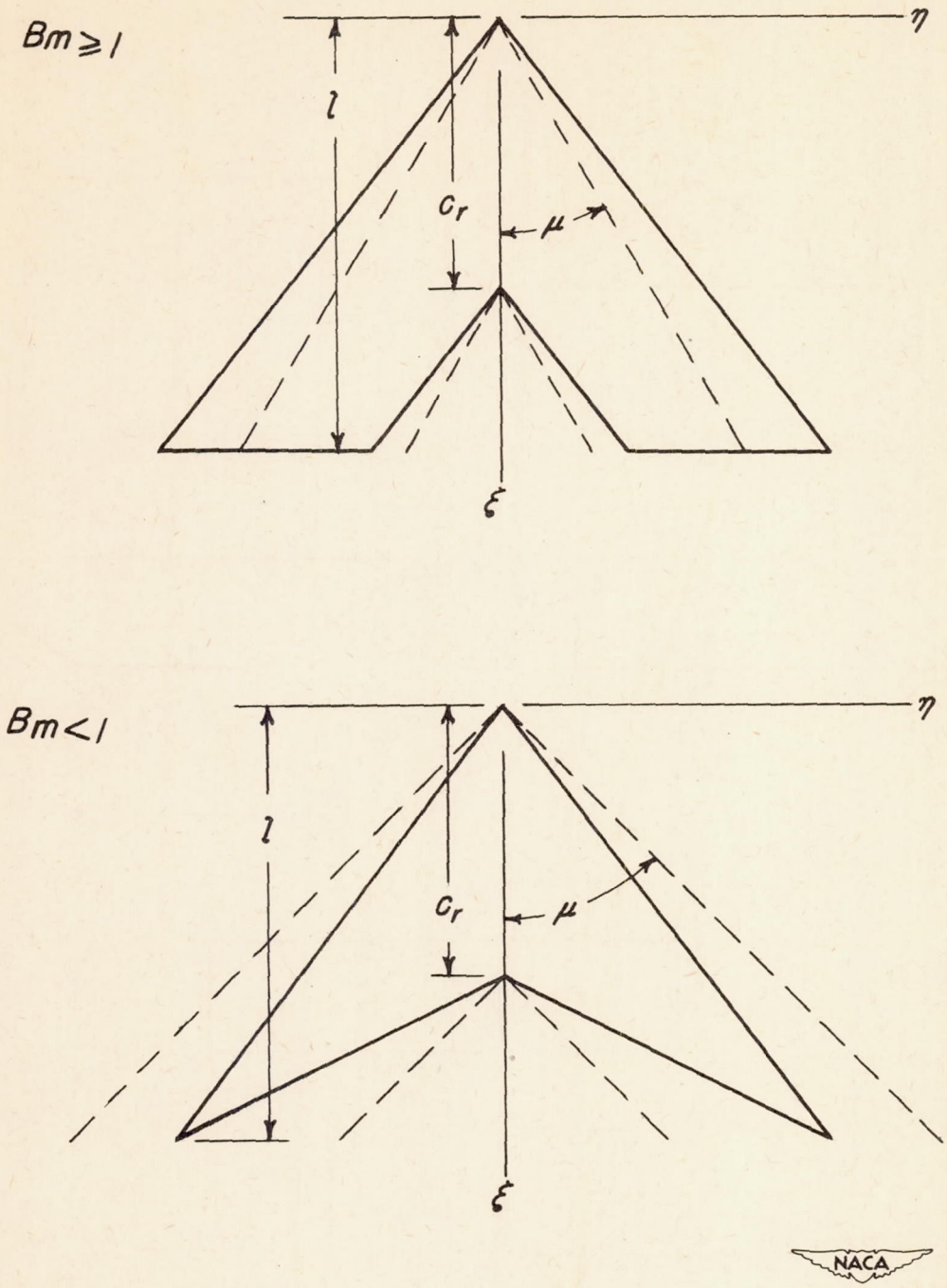


Figure 2.–Swept-back plan forms and Mach cone configurations investigated

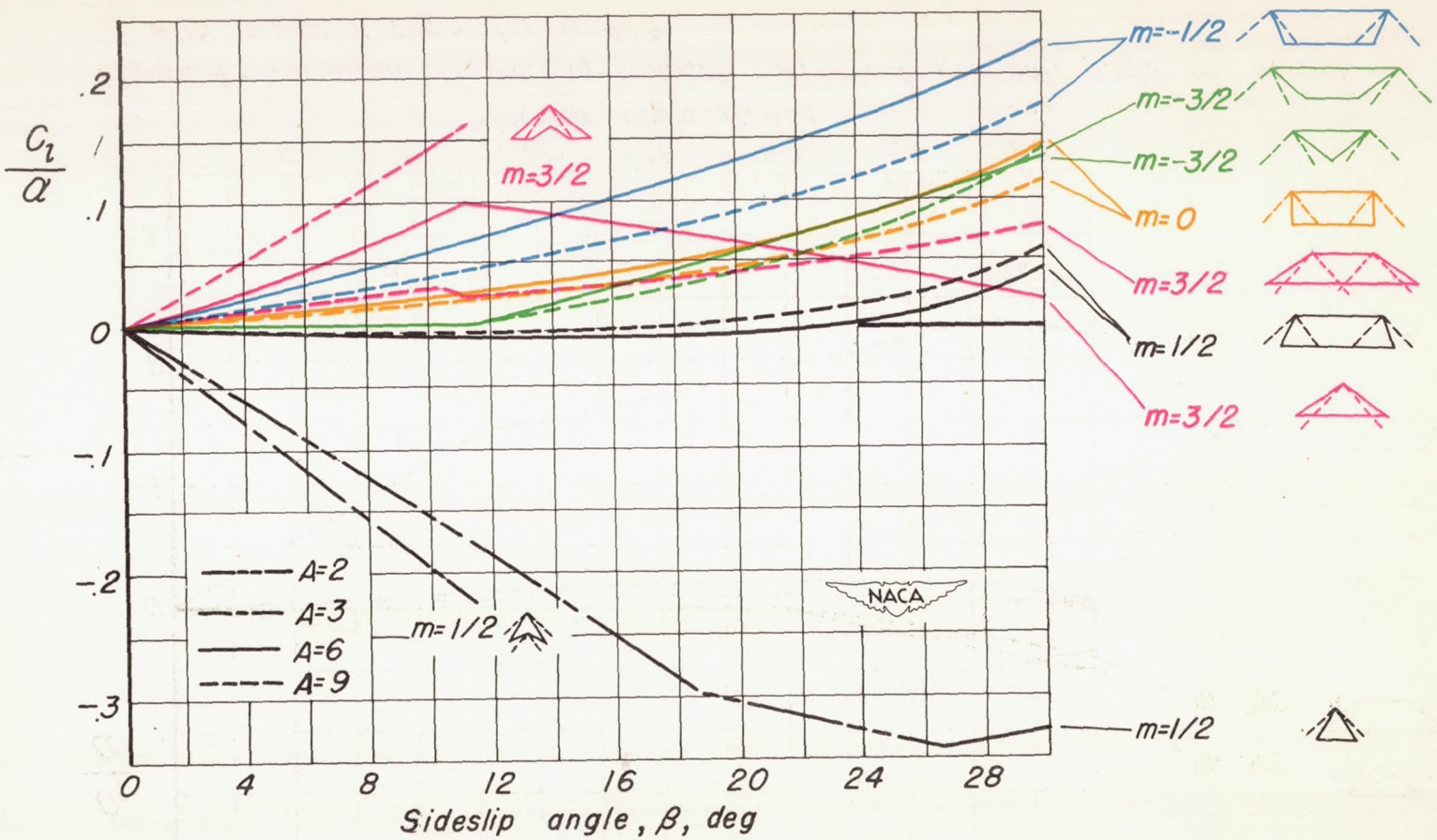


Figure 3.— Variation of rolling-moment coefficient per unit angle of attack with sideslip angle for B=1.

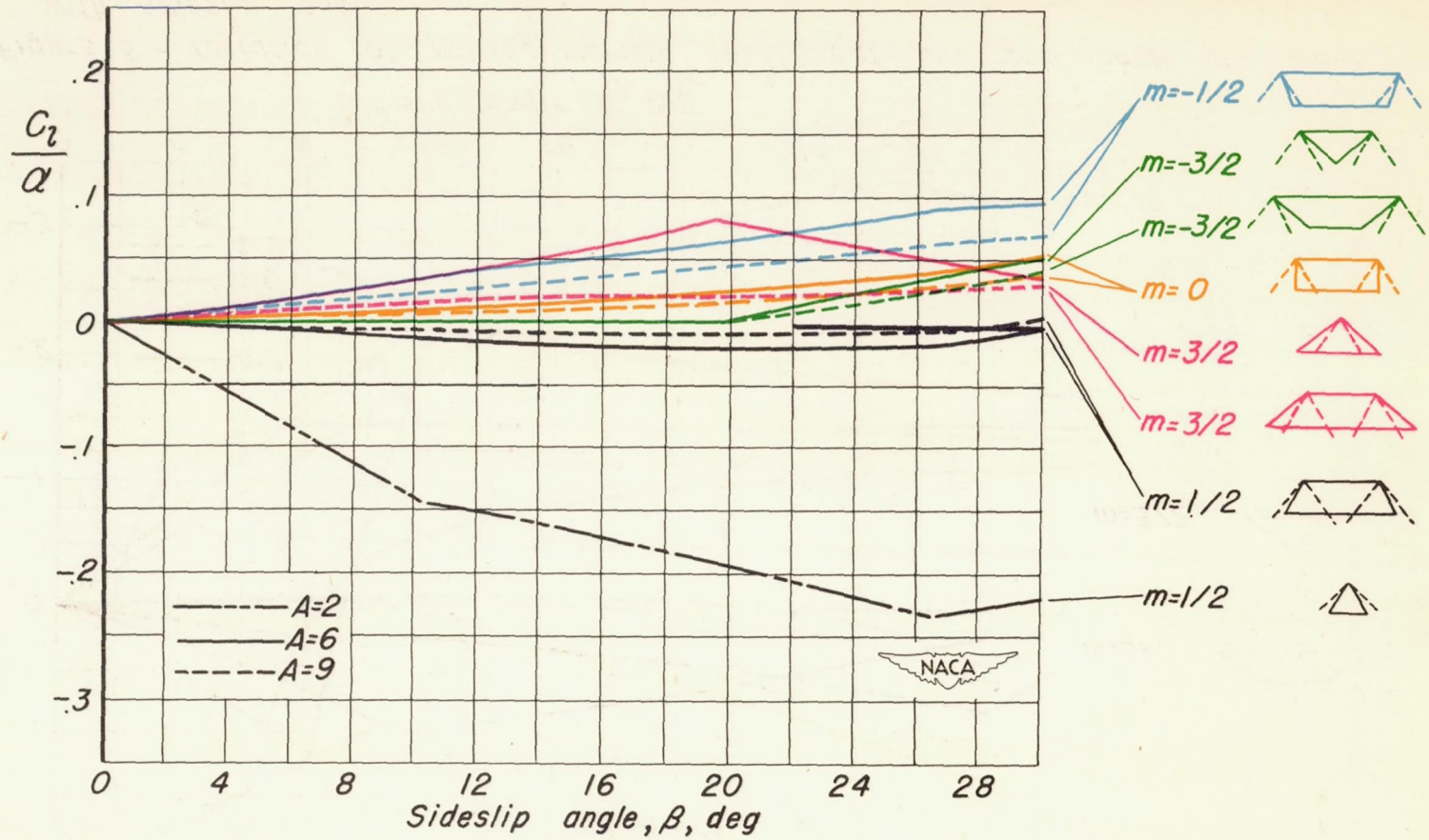


Figure 4.- Variation of rolling-moment coefficient per unit angle of attack with sideslip angle for B=4/3.

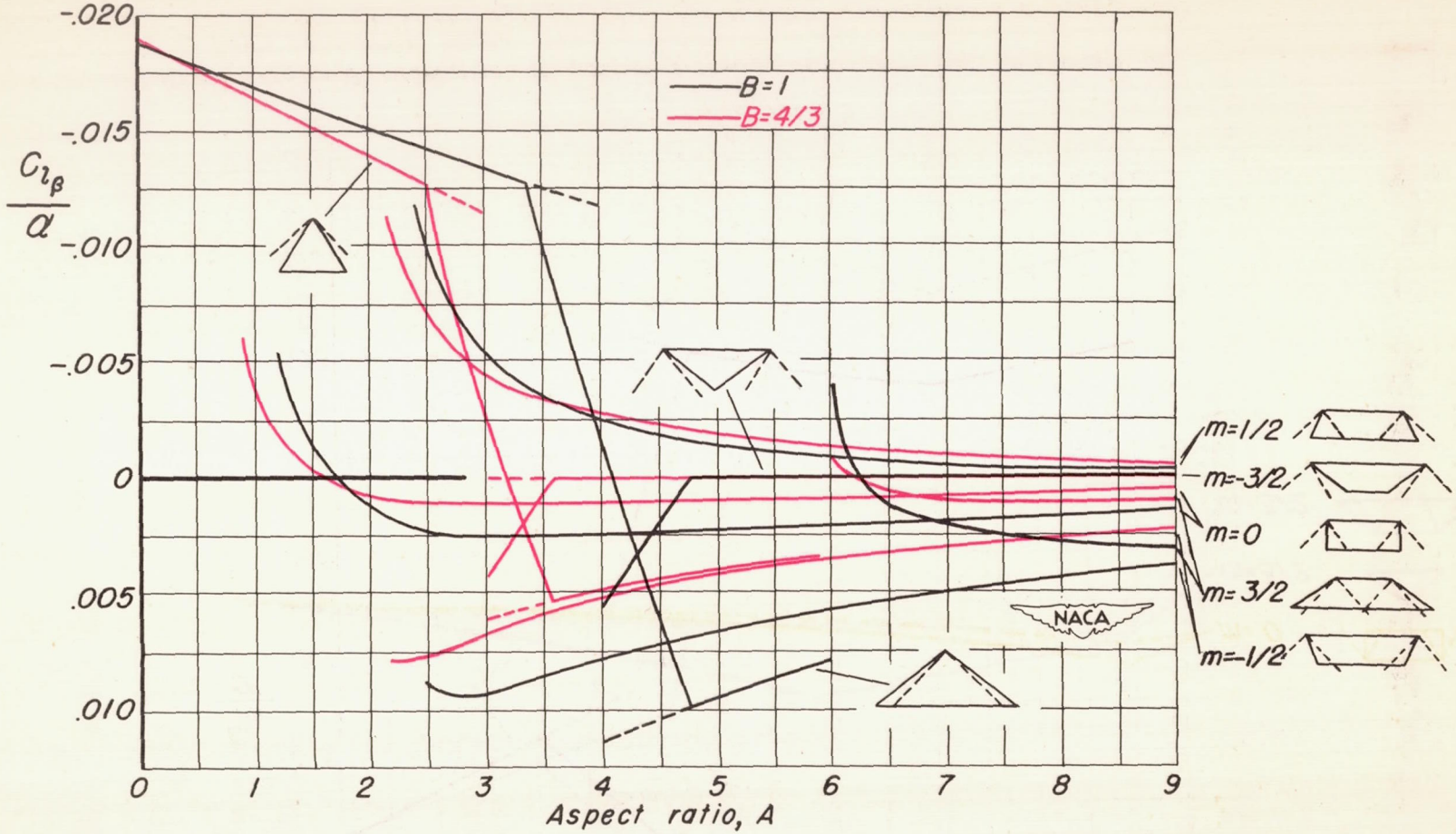


Figure 5 - Variation of roll-in-sideslip derivative per unit angle of attack with aspect ratio for typical triangular, trapezoidal, and rectangular plan forms; B=1 and B=4/3

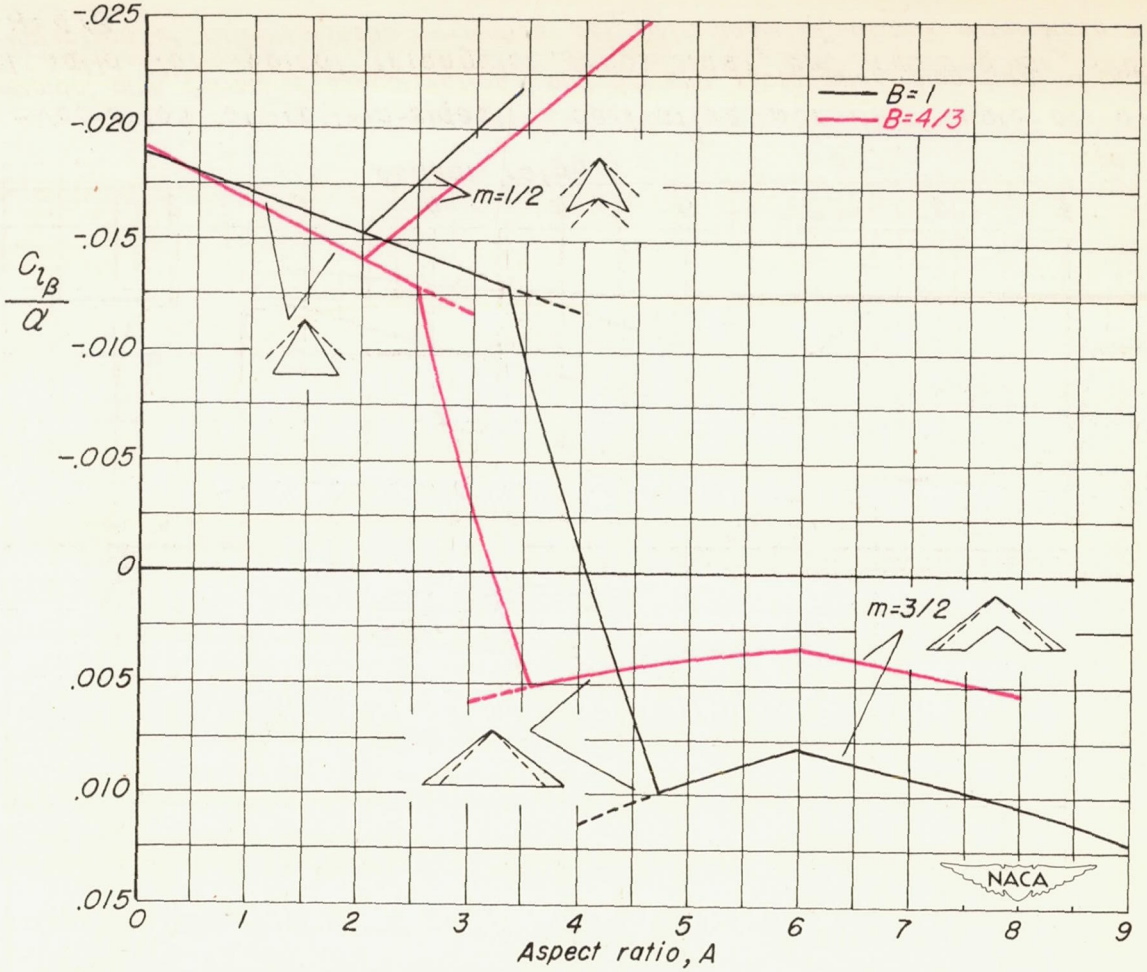
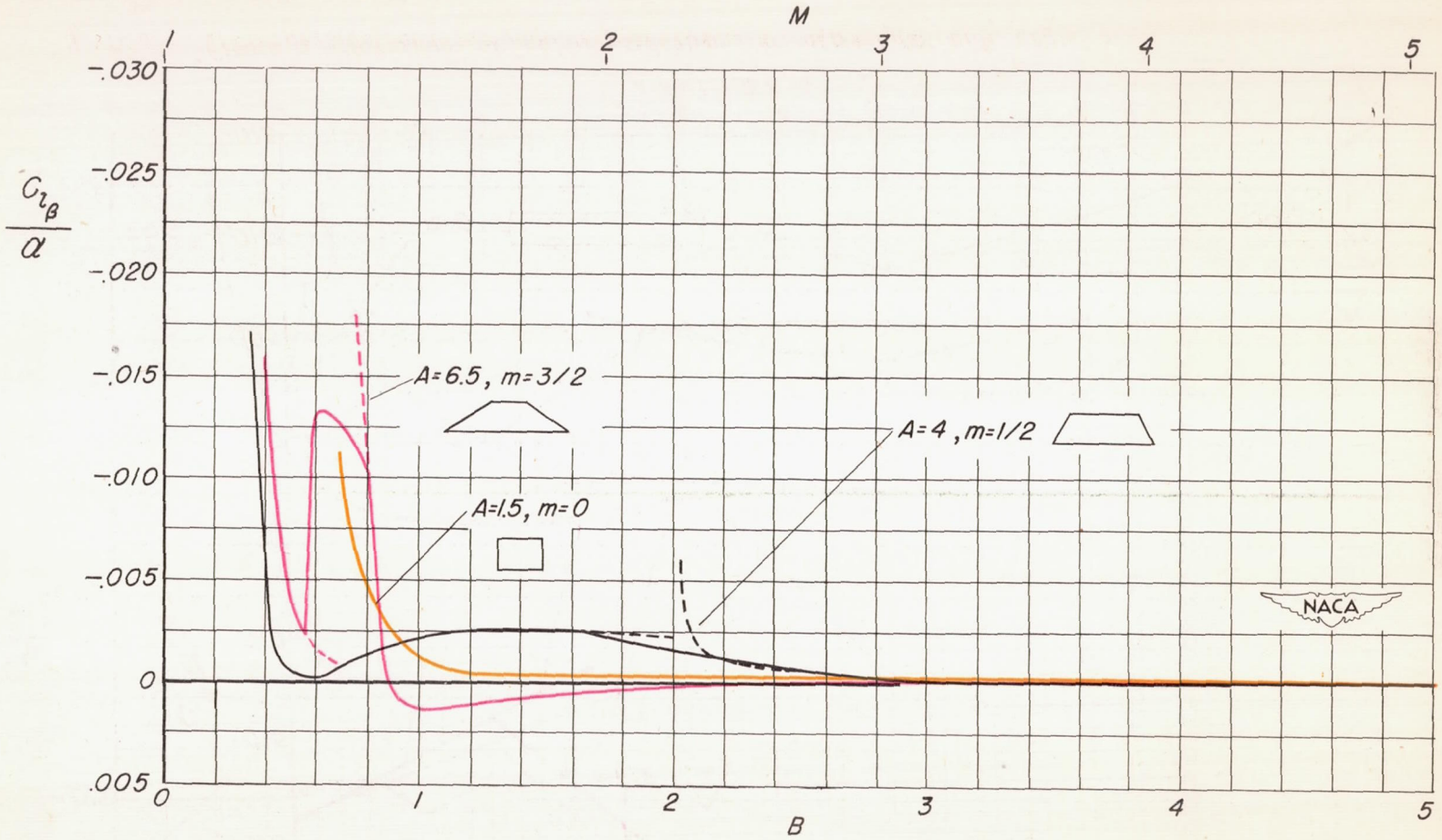
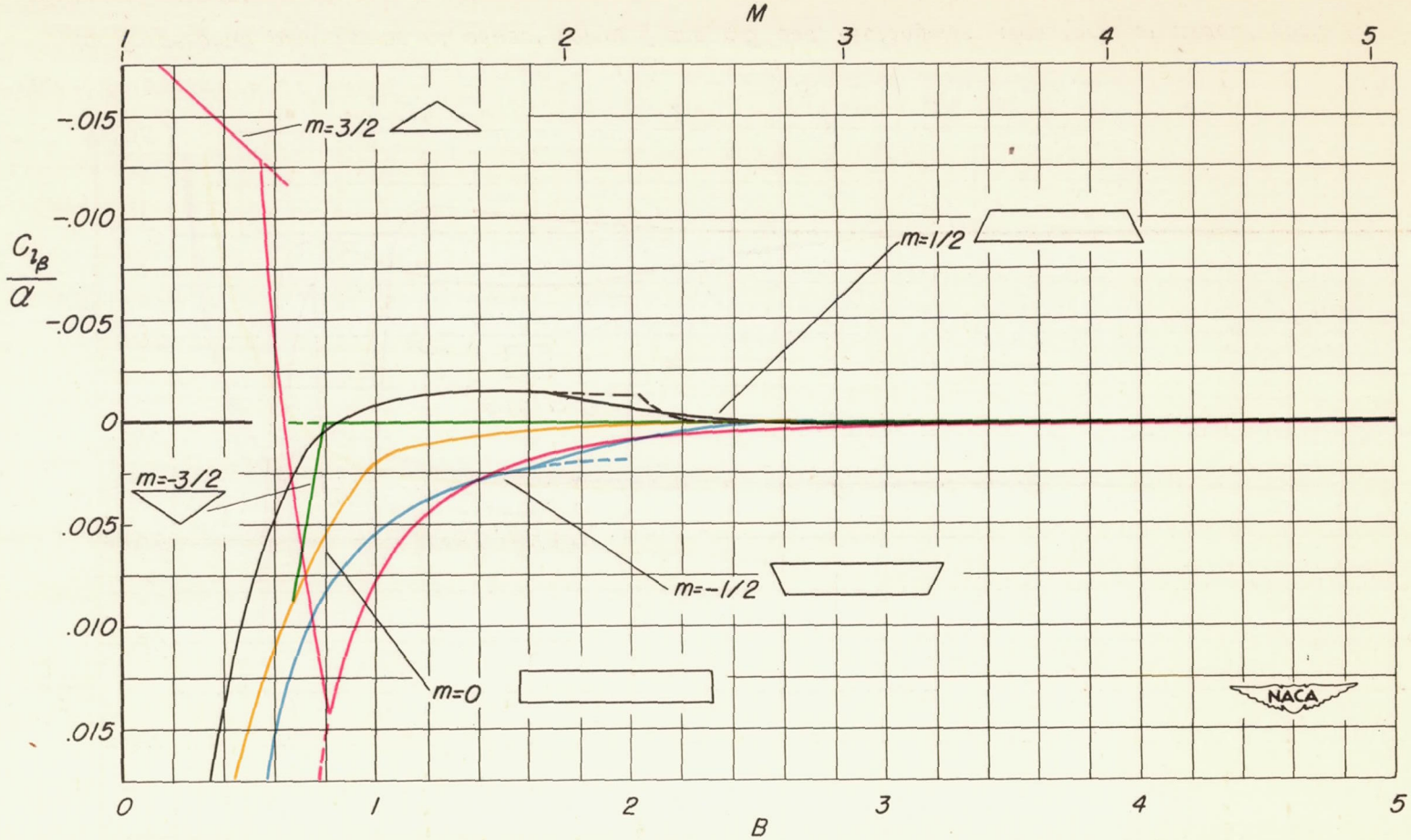


Figure 6 - Variation of roll-in-sideslip derivative per unit angle of attack with aspect ratio for typical triangular and swept-back plan forms; B=1 and B=4/3.



(a) Trapezoidal plan forms of aspect ratios 4 and 6.5 and rectangular plan form of aspect ratio 1.5

Figure 7- Variation of roll-in-sideslip derivative per unit angle of attack with Mach number parameter B.



(b) Triangular, trapezoidal, and rectangular plan forms of aspect ratio 6.

Figure 7.—Concluded

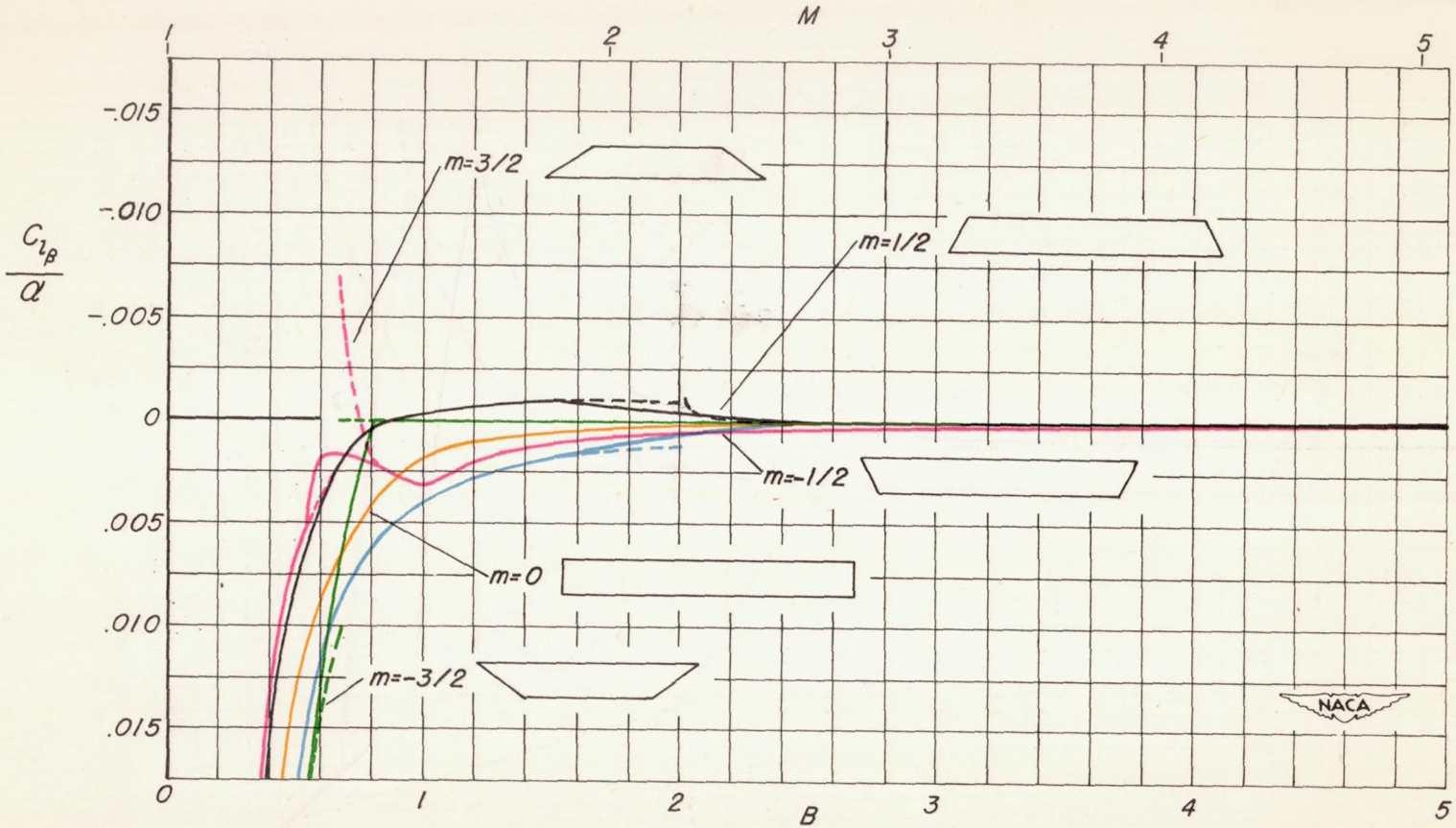


Figure 8 - Variation of roll-in-sideslip derivative per unit angle of attack with Mach number parameter B for typical trapezoidal and rectangular plan forms of aspect ratio 9.

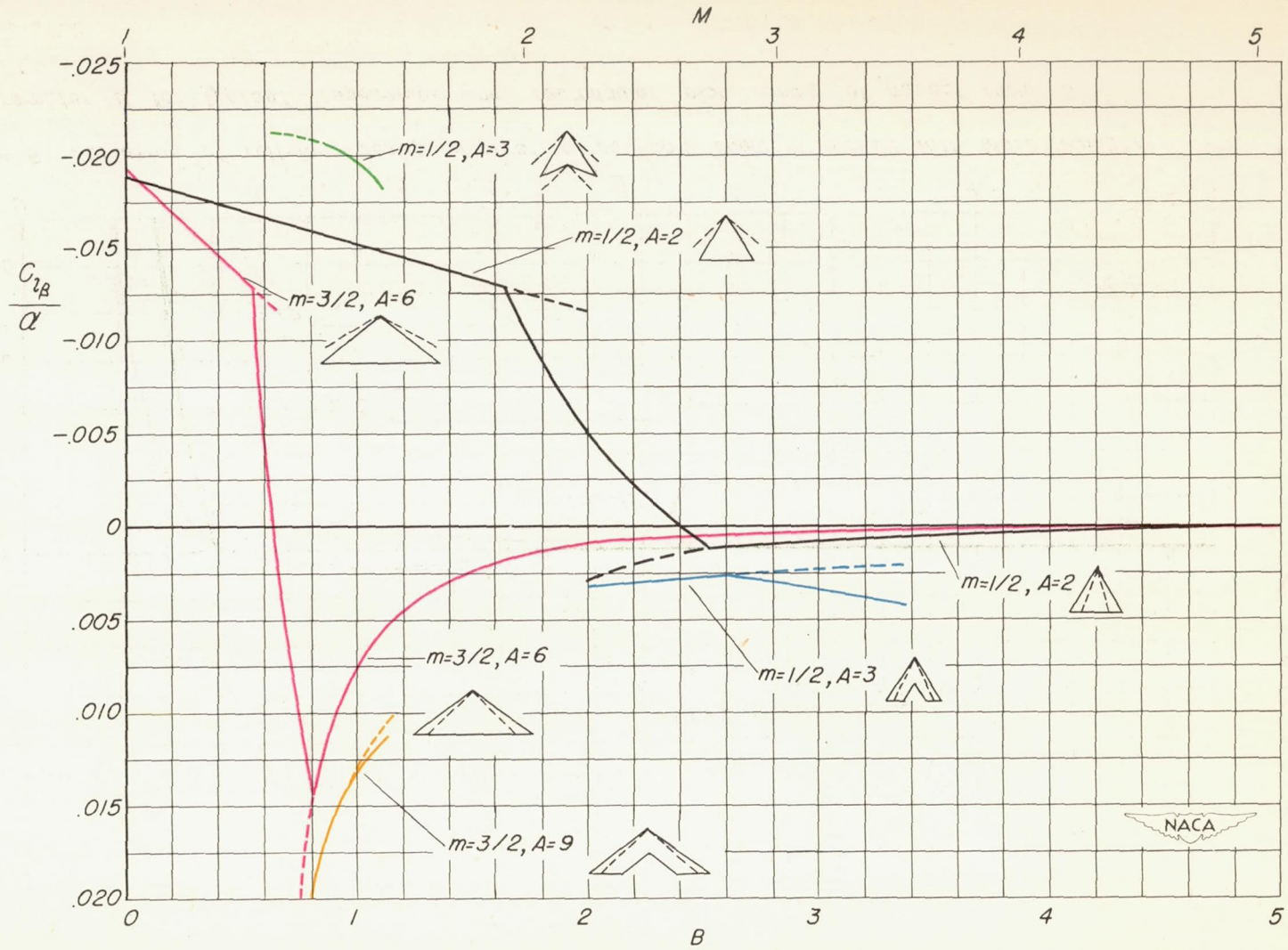


Figure 9.–Variation of roll-in-sideslip derivative per unit angle of attack with Mach number parameter B for typical triangular and swept-back plan forms.